Hydrodynamics of vegetated channels

Citation	Nepf, Heidi M. Hydrodynamics of Vegetated Channels. Journal of Hydraulic Research 50, no. 3 (June 2012): 262-279.
As Published	http://dx.doi.org/10.1080/00221686.2012.696559
Publisher	Taylor & Francis/International Association for Hydro-Environment Engineering and Research
Version	Author's final manuscript
Citable link	http://hdl.handle.net/1721.1/79045
Terms of Use	Creative Commons Attribution-Noncommercial-Share Alike 3.0
Detailed Terms	http://creativecommons.org/licenses/by-nc-sa/3.0/

Hydrodynamics of Vegetated Channels

Heidi M. Nepf
Department of Civil and Environmental Engineering
Massachusetts Institute of Technology
Cambridge, MA 02139, USA
hmnepf@mit.edu

Running Title: Vegetated Channels

Corresponding Author: Heidi M. Nepf
Department of Civil and Environmental Engineering
Massachusetts Institute of Technology
77 Massachusetts Avenue
Building 48-216D
Cambridge, MA 02139, USA
hmnepf@mit.edu
(617)-253-8622

Abstract:

This paper is a review of some recent studies in vegetation hydrodynamics, focusing on conditions within channels and spanning spatial scales from individual blades, to meadows, to the channel reach. At the blade-scale, the boundary layer formed on the plant surface plays a role in controlling nutrient uptake. Also, flow resistance and light availability are influenced by the reconfiguration of flexible blades. At the meadow-scale there are two flow regimes. For sparse meadows, the flow resembles a rough boundary layer. For dense meadows, the flow resembles a mixing layer. At the reach-scale, flow resistance is more closely connected to patch-scale vegetation distribution, described by the blockage factor, than to the geometry of individual plants. The impact of vegetation distribution on sediment movement is also discussed, with attention given to methods for estimating bed stress within regions of vegetation. To conclude, three examples are given to show how vegetation hydrodynamics plays an important role in the management of environmental systems; in channel restoration, flood management, and carbon cycling.

Introduction

Aquatic vegetation provides a wide range of ecosystem services. The uptake of nutrients and production of oxygen improves water quality (*e.g.* Chambers and Prepas 1994, Wilcock et al. 1999). The potential removal of nitrogen and phosphorous is so high that some researchers advocate widespread planting in waterways (Mars et al. 1999). Seagrasses are essential primary producers, forming the foundation of many food webs (Green & Short 2003), and in river channels vegetation promotes biodiversity by creating different habitat with spatial heterogeneity in the stream velocity (*e.g.* Kemp et al. 2000). Marshes and mangroves reduced coastal erosion by damping waves and storm surge (*e.g.* Brampton 1992, Turker et al. 2006, Othman 1994), and riparian vegetation enhances bank stability (Pollen and Simon 2005). Through the processes described above, aquatic vegetation provides ecosystem services with an estimated annual value of over ten trillion dollars (Costanza et al. 1997). These services are all influenced in some way by the flow field existing within and around the vegetated region.

In rivers, aquatic vegetation was historically considered only as a source of flow resistance, and vegetation was frequently removed to enhance flow conveyance and reduce flooding. Because of this context, the earliest studies of vegetation hydrodynamics focused on the characterization of flow resistance with a strictly hydraulic perspective (*e.g.* Ree 1949, Kouwen and Unny 1973, Kouwen 1990). However, as noted above, vegetation also provides ecological services that make it an integral part of coastal and river systems. To better understand and protect these systems, the study of vegetation hydrodynamics has, over time, become interwoven with other disciplines, such as biology (*e.g.* Hurd 2000, Koch 2001, Huang et al. 2011), fluvial geomorphology (e.g. Bennett et al. 2002, Tal and Paola 2007), landscape ecology (e.g. Larsen and Harvey 2011), and geochemistry (e.g. Clarke 2002, Harvey et al. 2003). This integration will surely accelerate in the future, as our discipline contributes to understanding and managing environmental systems.

The presence of vegetation alters the velocity field across several scales, ranging from individual branches and blades on a single plant, to the community of plants in a long meadow or finite length patch. Flow structure at the different scales is relevant to different processes. For example, the uptake of nutrients by an individual blade depends on the boundary layer on that blade, *i.e.* on the blade-scale flow (*e.g.* Koch 1994). Similarly, the capture of pollen is mediated by the flow structure generated around individual stigma (*e.g.* Ackerman 1997). In contrast, the retention or release of organic matter, mineral sediments, seeds, and pollen from a meadow of patch depends on the flow structure at the meadow- or patch-scale (*e.g.* Gaylord et al. 2004, Zong and Nepf 2010). Further, spatial heterogeneity in the meadow-scale parameters can lead to complex flow patterns. For example, in a marsh or wetland a branching network of channels cuts through regions of dense, largely emergent vegetation. While the channels provide most of the flow conveyance, the vegetated regions provide most of the ecosystem function and particle trapping. Thus, to describe marsh function one must describe the transport into and circulation within the vegetated regions. These examples tell us that to properly describe the physical role of vegetation within an environmental system, one must first identify the spatial scale relevant to a particular process, and choose models and measurements that are consistent with that scale. The following sections review some fundamental aspects of flow structure at the blade and meadow scale.

2. Flow at the scale of individual blades

2.1 Blade Boundary Layers and Nutrient Fluxes

At the scale of individual blades and leaves, the hydrodynamic response is dominated by boundary layer formation on the plant surface. A flat plate has often been used as a model for flow adjacent to blades and leaves oriented in the streamwise (x) direction (Figure 1). A viscous boundary layer forms at the leading edge ($x = 0$) of the blade, and its thickness, δ, grows with streamwise distance, specifically, $\delta(x) = 5\sqrt{\nu x/U}$, with U the mean current and ν the kinematic viscosity (*e.g.* White 2008). As the viscous boundary layer grows thicker, it becomes sensitive to perturbations caused by turbulent oscillations in the outer flow or by irregularities in surface texture. At some point along the blade the boundary layer transitions to a turbulent boundary layer with a viscous sub-layer, δ_s (Figure 1). The transition occurs near $Re_x = Ux/\nu \approx 10^5$, but can be modified by surface roughness (White, 2008). If the length of the blade is less than the transition length, $x_t = 10^5 \nu/U$, the boundary layer is laminar over the entire blade. If the boundary layer becomes turbulent, the viscous sub-layer will have a constant thickness set by the friction velocity on the blade, u_{b*}. Experiments and scaling indicate that the viscous sub-layer is between $\delta_s = 5\nu/u_{b*}$ and $10\nu/u_{b*}$ (*e.g.* Kundu and Cohen 2002, Boudreau and Jorgensen 2001). Within this layer the flow is essentially laminar.

Because of the difference in molecular diffusivity, the concentration boundary layer, δ_c, is smaller than the momentum boundary layer, δ_s. Specifically, $\delta_c = \delta_s\, Sc^{-1/3}$, with Schmidt number $S_c = \nu/D_m$ and molecular diffusivity D_m (*e.g.* Boudreau and Jorgensen 2001). The kinematic viscosity of water is of the order $\nu = 10^{-6}$ m^{2}s^{-1} and for most dissolved species D_m is of the order 10^{-9} m^{2}s^{-1}, so that, in water we generally find $\delta_c = 0.1\ \delta_s$. Within δ_c transport perpendicular to the surface can only occur through molecular diffusion, so that this layer is also called the diffusive sub-layer.

The mass flux at the surface, $\dot{m}$, is described by Fick's Law (*e.g.* Kays and Crawford, 1993).

$$\frac{\dot{m}}{A} = -D_m \frac{\partial C}{\partial n_\perp} \tag{1}$$

Here, A is the surface area, and $\partial C/\partial n_\perp$ is the gradient in concentration perpendicular to the surface. It is often assumed that the flux across δ_c is the rate-limiting step in transferring dissolved species to the blade surface. In this case, the concentration at the surface is assumed to be zero, *i.e.* the plant is a perfect absorber, taking in each molecule the instant it reaches the surface. In addition, because transport across the sub-layer proceeds at the rate of molecular diffusion, it is several orders of magnitude slower than the turbulent diffusion occurring outside this layer. Therefore, it is reasonable to assume that the concentration at the outer edge of the sub-layer is the bulk fluid concentration C. Then, $\partial C / \partial n_{\perp} \approx C/\delta_c$, and (1) can be reduced to (*e.g.* Boudreau and Jorgensen 2001),

$$\dot{m} = \frac{D_m A C}{\delta_c} = \frac{u_*}{10\nu} Sc^{1/3} D_m A C \sim U\,, \tag{2}$$

where we have used the relations for δ_c introduced above. Equation (2) suggests that the uptake rate increases with increasing velocity, U. Several studies have captured this behavior for nutrient uptake by seagrasses (*e.g.* Koch 1994, Thomas et al. 2000). However, as the velocity increases, at some point the physical rate of mass flux matches and then surpasses the biological rate of incorporation at the blade surface. At this point the uptake rate is controlled biologically, and this is called the biologically-limited flux rate. This transition was observed to occur around $U = 8$ *cm/s* for *Macrocystis integrifolia* blades (Hurd et al. 1996), and around $U = 4$ and 6 cm/s for *Thalassia testudinum* and *Cymodocea nodosa*, respectively (Koch 1994). The transition velocity depends on the biological rate, which in turn depends on light availability and temperature (Koch 1994).

A flat plate is not always a good geometric model for a plant surface. However, a generalized version of (2) will hold for surfaces of any shape or rigidity, and mass-transport limitation by a diffusive sub-layer can occur on any surface. Specifically, the mass-flux can be described at any point on the surface by $\dot{m} = D_m A C / \delta_c$. The problem lies in describing the sub-layer thickness, δ_c, which can vary along the surface due to changes in surface texture, and due to the surface shape. For example, on an undulated blade of the kelp *Macrocystis integrifolia*, the laminar sub-layer is thinned at the apex of each undulation, and thickened on the downstream side, relative to a flat blade under the same mean flow conditions (Hurd et al. 1997). Further, blade motion may disturb the diffusive sub-layer, replacing the fluid next the surface with fluid from outside the boundary layer, which in turn creates an instantaneously higher concentration gradient at the surface and thus higher fluxes (*e.g.* Koehl and Alberte 1988, Hurd 2000, Denny and Roberson 2002). This process can be represented by the surface renewal model (Stevens et al. 2003, Huang et al. 2011). Recent studies have documented blade motions associated with turbulence (Plew *et al*. 2008, Siniscalchi e*t al*. 2012), and future studies should examine how the turbulence-induced motion may enhance flux.

2.2 Flexibility and Reconfiguration

Because many aquatic plants are flexible, they can be pushed over by currents, resulting in a change in morphology called reconfiguration (*e.g.* Vogel, 1994). The change in blade posture can alter light availability in two competing ways. When a blade is pushed over, its horizontal projected area increases, creating a larger surface area for light interception, but the greater horizontal projection also increases shading among neighboring bladesm which would tend to reduce light interception (Zimmerman 2003). Reconfiguration also reduces flow resistance through two mechanisms. First, reconfiguration reduces the frontal area of the vegetation, and second, the reconfigured shape tends to be more streamlined (de Langre 2008). Because of reconfiguration, the drag on a plant increases more slowly with velocity, than predicted by the quadratic law. To quantify this deviation from the quadratic law, the relationship between the drag force (*F*) and velocity (*U*) has been expressed as $F \propto U^{2+\gamma}$, with γ called the Vogel exponent. The Vogel exponent has been observed to vary between $\gamma = 0$ (rigid) and $\gamma = -2$ (very flexible) for aquatic species (Vogel, 1994).

In practice, predictions of drag have used the standard quadratic law, but allow the reference area and drag coefficient to vary with velocity. There has been significant debate about which reference area (*e.g.* frontal area) best characterizes drag as the vegetation is pushed over (see discussion of Sand-Jensen 2003 by Green 2005a; Sukhodolov 2005; Statzner et al. 2006). Some recent studies have addressed this debate by developing drag relationships that incorporate the change in posture (*e.g.* Luhar and Nepf 2011).

A flexible body in flow will adjust its shape until there is a balance between the drag force and the restoring force due to body stiffness, for which scaling predicts $F \propto U^{4/3}$ (*e.g.* Alben et al. 2002, Gosselin et al. 2010, de Langre 2008). Because many aquatic species have gas-filled sacs or material density less than water, buoyancy may also act as a restoring force. Green (2005) and Abdelrhman (2007) developed models for plant posture that consider only buoyancy. Dijkstra and Uittenbogaard (2010) and Luhar and Nepf (2011) considered both buoyancy and rigidity, in which case reconfiguration depends on two dimensionless parameters that represent the ratios of forces associated with drag, rigidity and buoyancy. The Cauchy number, *Ca*, is the ratio of drag and the stiffness restoring force. The buoyancy parameter, *B*, is the ratio of the restoring forces due to buoyancy and stiffness. For a blade of length *l*, width *b*, thickness *t*, and density, ρ_v, and in a uniform flow of horizontal velocity *U*, these parameters are defined as:

$$B = \frac{(\rho - \rho_v) g b t l^3}{EI} \qquad (3)$$

$$Ca = \frac{1}{2}\frac{\rho C_D b U^2 l^3}{EI} \qquad (4)$$

Here, E is the elastic modulus for the blade, $I(=bt^3/12)$ is the second moment of area, ρ is the density of water, and g is the acceleration due to gravity.

As an alternative to empirically determined drag coefficients, $C_D = f(U)$, Luhar and Nepf (2011) proposed an effective blade length, l_e, to describe the impact of reconfiguration on drag. The effective blade length is defined as the length of a rigid, vertical blade that generates the same horizontal drag as the flexible blade of total length l. Based on this definition, the horizontal drag force on the blade is $F_x = (1/2)\rho C_D b l_e U^2$, where the drag coefficient, C_D, for the flexible blades is identical to that for rigid, vertical blades. The following relationships for effective length, l_e, and meadow height, h, are based on the model described in Luhar and Nepf (2011, 2012).

$$\frac{l_e}{l} = 1 - \frac{1 - 0.9Ca^{-1/3}}{1 + Ca^{-3/2}(8 + B^{3/2})} \qquad (5)$$

$$\frac{h}{l} = 1 - \frac{1 - Ca^{-1/4}}{1 + Ca^{-3/5}\left(4 + B^{3/5}\right) + Ca^{-2}\left(8 + B^{2}\right)} \qquad (6)$$

When rigidity is the dominant restoring force ($Ca >> B$), (6) reduces to $h/l \sim Ca^{-1/4} \sim (EI/U^2)^{1/4}$, which is similar to the scaling suggested by Kouwen and Unny (1973) and later by Velasco et al. (2003). Although (5) and (6) were developed for individual blades, Luhar and Nepf (2012) demonstrate how they can be used to predict the height (h) of a submerged meadow, and how the predicted h and l_e can then be used to predict channel-scale resistance.

3. Uniform Meadows of Submerged Vegetation

In this section we consider a community of individual plants within a uniform, submerged meadow. The flow at the meadow scale is less dependent on the specific morphology of each plant or blade, but responds instead to the average flow resistance associated with the distribution of meadow elements. The meadow geometry is defined by the scale of individual stems and blades, and the number of these elements per bed area. If the individual stems or blades have a characteristic diameter or width d, and an average spacing ΔS, then the frontal area per volume within the meadow is $a = d/\Delta S^2$. Note that a can only be properly defined as an average of a length-scale greater than ΔS, and by using this representation for meadow geometry we forfeit the resolution of flow structure at scales less than ΔS. The meadow density can also be described by the solid volume fraction occupied by the canopy elements, ϕ, or the porosity, $n = (1-\phi)$. If the individual elements approximate a circular cylinder, *e.g.* reed stems, then $\phi = (\pi/4)\, ad$. If the morphology is strap-like, with blade width d and thickness b, then $\phi = db/\Delta S^2 = ab$. Note that d and ΔS, and therefore a, can vary spatially within the meadow, and specifically over the height of the meadow. In addition, for flexible vegetation, the posture of the blades is influenced by the flow (see discussion in 2.1). As flow speed increases, individual blades are pushed over into more streamlined positions. As the meadow becomes more compressed (decreased meadow height) with increasing flow speed, both a and ϕ increase. Finally, a non-dimensional measure of the canopy density is the frontal area per bed area, λ, known as the roughness density (Wooding, Bradley & Marshall 1973). For meadow height h, and $z = 0$ at the bed,

$$\lambda = \int_{z=0}^{h} a\,dz = ah \qquad (7)$$

with the right-most expression valid for vertically uniform *a*.

Within a canopy, flow is forced to move around each branch or blade, so that the velocity field is spatially heterogeneous at the scale of these elements. A double-averaging method is used to remove the element-scale spatial heterogeneity, in addition to the more common temporal averaging (Gray & Lee 1977; Raupach & Shaw 1982, Nikora 2007 and references therein). The velocity vector $\vec{u} = (u, v, w)$ corresponds to the coordinates (*x, y, z*), respectively. The instantaneous velocity and pressure (*p*) fields are first decomposed into a time average (overbar) and deviations from the time-average (single prime). The time-averaged quantities are further decomposed into a spatial mean (angle bracket) and deviations from the spatial mean (double prime). The spatial averaging volume is thin in the vertical, to preserve vertical variation in meadow density, and large enough in the horizontal plane to include several stems ($> \Delta S$).

Applying this averaging scheme to a homogeneous canopy, the momentum equation in the stream-wise direction is (*e.g*. Nikora et al. 2007).

$$\frac{D\langle\bar{u}\rangle}{Dt} = g\sin\theta - \frac{1}{n\rho}\frac{\partial n\langle\bar{p}\rangle}{\partial x} \underbrace{- \frac{1}{n}\frac{\partial}{\partial z} n\langle\overline{u'w'}\rangle}_{\text{(i)}} \underbrace{- \frac{1}{n}\frac{\partial}{\partial z} n\langle\bar{u}''\bar{w}''\rangle}_{\text{(ii)}} \underbrace{+ \frac{1}{n}\nu\frac{\partial}{\partial z} n\frac{\partial\langle\bar{u}\rangle}{\partial z}}_{\text{(iii)}} - D_x \qquad (8)$$

Here, θ is the bed slope. Term (i) is the spatial-average of the Reynolds' stress. Term (ii), called the dispersive stress, is the momentum flux associated with spatial correlations in the time-averaged velocity field. Poggi et al. (2004b) show that the dispersive stress is less than 10% of the Reynolds stress (i) for $\lambda = ah > 0.1$. Term (iii) is the viscous stress associated with the spatial variation in $<\bar{u}>$. The final term, D_x, is the spatially-averaged drag associated with the canopy elements, which is often represented by a quadratic drag law (*e.g*. Kaimal & Finnegan 1994, p. 95).

$$D_x = \frac{1}{2}\frac{C_D a}{n}\langle\bar{u}\rangle\left|\langle\bar{u}\rangle\right| \qquad (9)$$

The canopy-drag length-scale, L_c, is defined from the quadratic drag law. Based on dimensional reasoning $D_x = \langle \bar{u} \rangle^2 / L_c$ (Belcher et al. 2003). From (9)

$$L_c = \frac{2(1-\phi)}{C_D a}. \tag{10}$$

This represents the length-scale over which the mean and turbulent flow components adjust to the canopy drag. Since, most aquatic canopies have high porosity ($\phi < 0.1$), this scale is commonly approximated by $2(C_D a)^{-1}$.

3.1 Stem-scale turbulence

Branches and stems with an orientation that is perpendicular to the flow can generate turbulence. The stem diameter (or blade width) d defines the stem Reynolds' number, $Re_d = Ud/\nu$. For $Re_d > \approx 100$, the canopy elements will generate vortices of scale d, which is called stem-scale turbulence (*e.g*. Nepf 2012 and references therein). If the stem density is high, such that the mean spacing between stems (ΔS) is less than d, the turbulence is generated at the scale ΔS (Tanino and Nepf 2008). Even for very sparse canopies, the production of turbulence within stem wakes is comparable to or greater than the production by bed shear (Nepf *et al.* 1997, Burke & Stolzenbach 1983, Lopez & Garcia 1998). Therefore, turbulence level *cannot* be predicted from the bed-friction velocity, as it is for open-channel flow. Instead, it is a function of the canopy drag. Vortex generation in stem wakes drains energy from the mean flow (expressed as mean canopy drag) and feeds it into the turbulent kinetic energy. If this conversion is 100% efficient, then the rate at which turbulent energy is produced is equal to the rate of work done by the flow against canopy drag (Raupach and Shaw 1982). If we further assume that the energy is extracted at the length-scale ℓ, the turbulent kinetic energy (k) in the canopy may be estimated from (Tanino and Nepf 2008),

$$\frac{\sqrt{\langle \bar{k} \rangle}}{\langle \bar{u} \rangle} \approx \left(C_D \frac{\ell}{d} \frac{2\phi}{(1-\phi)\pi} \right)^{1/3}. \tag{11}$$

Here, ℓ is the smaller of d or ΔS. In fact, only the form drag is converted into turbulent kinetic energy. The viscous drag is dissipated directly to heat. For stiff canopies, or near the rigid base of most stems, the drag is mostly form drag, and (11) is a reasonable approximation. However, in the streamlined portion of flexible submerged plants the drag is predominantly viscous, and (11) would be an overestimate of stem-scale turbulence production (Nikora & Nikora 2007).

An interesting non-linear behavior emerges when we compare conditions of different stem density under the same driving force (*i.e.* the same potential and/or pressure gradient). The details of this comparison are given in Nepf (1999). Because the vegetation offers resistance to flow, the velocity within a meadow is always less than the velocity over a bare bed under the same external forcing, and the canopy velocity decreases monotonically with increasing stem density (or ϕ). However, changes in turbulent kinetic energy, $<\bar{k}>$, reflect competing effects as stem density (ϕ) increases, *i.e.* turbulence intensity, $<\bar{k}>/<\bar{u}>^2$, increases, but $<\bar{u}>^2$ decreases, which together produce a non-linear response. As stem density (or ϕ) increases from zero, $<\bar{k}>$ initially increases, but eventually decreases as ϕ increases further. This non-linear response was predicted numerically for flow through emergent vegetation (Burke and Stolzenbach, 1983) and within submerged roughness elements (Eckman, 1990). It was also observed in a flume study of *Zostera Marina*

(Gambi *et al*., 1990). The fact that at some stem densities the near bed turbulence level within a meadow can be higher than over adjacent bare bed has important implications for sediment transport. This is discussed further in the next section.

3.2 Sparse and Dense Meadows

We now consider a submerged meadow of height h in water of depth H (Figure 2). For a submerged meadow, there are two limits of flow behavior, depending on the relative importance of the bed shear and meadow drag. If meadow drag is small compared to bed drag, then the velocity follows a turbulent boundary layer profile, with the vegetation contributing to the bed roughness. This regime is called a sparse meadow or canopy (Figure 2a). In this regime, the turbulence near the bed will increase as stem density increases. Alternatively, in the dense canopy regime the meadow drag is large compared to the bed stress, and the discontinuity in drag at the top of the meadow generates a region of shear resembling a free-shear-layer and notably including an inflection point near the top of the meadow (Figure 2b, c). From scaling arguments, the transition between sparse and dense regimes occurs at $\lambda = ah = 0.1$ (Belcher et al 2003). From measured velocity profiles, a boundary-layer form with no inflection point is observed for $C_D ah < 0.04$, and a pronounced inflection point appears for $C_D ah > 0.1$ (Nepf et al 2007). Since $C_D \approx 1$ the measured and theoretical limits are consistent.

If the velocity profile contains an inflection point, it is unstable to the generation of Kelvin-Helmoltz (KH) vortices (*e.g*. Raupach et al 1996). These structures dominate the vertical transport at the canopy interface (*e.g*. Gao et al. 1989, Finnigan 2000, Ghisalberti & Nepf 2002). These vortices are called canopy-scale turbulence, to distinguish it from the much-larger boundary-layer turbulence, which may form above a deeply submerged or unconfined canopy, and the much smaller stem-scale turbulence. Over a deeply submerged (or terrestrial) canopy ($H/h > 10$), the canopy-scale vortices are highly three-dimensional due to their interaction with the boundary-layer turbulence, which stretches the canopy-scale vortices, enhancing secondary instabilities (Fitzmaurice et al. 2004, Finningan et al 2009). However, with shallow submergence ($H/h <= 5$), which is common in aquatic systems, larger-scale boundary-layer turbulence is not present, and the canopy-scale vortices dominate the turbulence both within and above the meadow (Ghisalberti & Nepf 2005, 2009).

Within a distance of about $10h$ from the canopy's leading edge, the canopy-scale vortices reach a fixed scale and a fixed penetration into the canopy (δ_e in Figure 2, Ghisalberti 2000, Ghisalberti & Nepf 2000, 2004, 2009). The final vortex and shear-layer scale is reached when the shear-production that feeds energy into the canopy-scale vortices is balanced by the dissipation by canopy drag. This balance predicts the following scaling, which has been verified with observations (Nepf et al. 2007).

$$\delta_e = \frac{0.23 \pm 0.6}{C_D a} \qquad (12)$$

Recall that $C_D ah \geq 0.1$ is required to produce shear-layer vortices, so that (12) applies only to those canopies. In the range $C_D ah = 0.1$ to 0.23, the shear-layer vortices penetrate to the bed, $\delta_e = h$, creating a highly turbulent condition over the entire canopy height (Figure 2b). At higher values of $C_D ah$ the canopy-scale vortices do not penetrate to the bed, $\delta_e < h$ (Figure 2c). If the submergence ratio $H/h < 2$, δ_e is diminished from (12), as interaction with the water surface diminishes the strength and scale of the vortices (Nepf & Vivoni 2000, Okamoto & Nezu 2009).

The penetration length, δ_e, segregates the canopy into an upper layer of strong turbulence and rapid renewal and a lower layer of weak turbulence and slow renewal (Nepf & Vivoni 2000, Nepf et al 2007). Flushing of the upper canopy is enhanced by the canopy-scale vortices that penetrate this region. In contrast, turbulence in the lower canopy ($z < h - \delta_e$) is generated in stem wakes and has significantly smaller scale, set by the stem diameters and spacing. Canopies for which $\delta_e/h < 1$ (Figure 2c) shield the bed from strong turbulence and turbulent stress. Because turbulence near the bed plays a role in resuspension, these dense canopies are expected to reduce resuspension and erosion. Consistent with this, Moore (2004) observed that resuspension within a seagrass meadow was reduced, relative to bare-bed conditions, only when the above ground biomass per area was greater than 100 g/m^2 (dry mass). This biomass corresponds to $ah = 0.4$ (Luhar et al. 2008). In a similar study, Lawson et al (2012) measured sediment erosion in beds of different stem density. Using the blade length (8 cm) and width (3mm) provided in that paper, we convert the stem density into a roughness density *ah*. Between 80 and 300 stems m^{-2} ($ah = 0.02$ to 0.07) erosion increased with increasing stem density, consistent with sparse canopy behavior, *i.e.* stem-scale turbulence augmented the near-bed turbulence, and increased with increasing stem density. However, above 500 stems m^{-2} ($ah = 0.12$) bed erosion was essentially eliminated within the meadow (Lawson et al. 2012). Both the Moore and Lawson studies demonstrate a stem density threshold, above which the near bed turbulence becomes too weak to generate resuspension and erosion. The threshold is roughly consistent with the roughness density transition suggested by (12) and depicted in Figure 2.

The regimes depicted in Figure 2 give rise to a feedback between optimum meadow density and substrate type. Because dense canopies reduce near-bed turbulence, they promote sediment retention. In sandy regions, that tend to be nutrient poor, the preferential retention of fines and organic material, *i.e.* muddification, enhances the supply of nutrient to the canopy, so that dense canopies provide a positive feedback to canopy health in sandy regions (*e.g.* van Katwijk et al 2010). In contrast, in regions with muddy substrate, which is more susceptible to anoxia, sparse meadows ($C_Dah \leq 0.1$) may be more successful, because the enhanced near-bed turbulence removes fines, leading to a sandier substrate that is less prone to anoxia.

Both the boundary layer profile of a sparse canopy regime and the mixing layer profile of the dense canopy regime have been observed in the field, in seagrass meadows (Lacy 2011) and in river meadows (Sukhodolov and Sukhodolova 2010). Although both profiles have been observed in the field, modeling efforts have focused on the dense canopy limit. Most methods divide the flow into a uniform layer within the vegetation and a logarithmic profile above the vegetation. Given the poor scale-separation between plant height and flow depth, it is unlikely that a genuine logarithmic layer exists in aquatic flows over vegetation. However, previous studies have shown that a logarithmic profile provides a reasonable description of the velocity above a meadow for $H/h > 1.5$ (*e.g.* Nepf and Vivoni 2000, Poggi et al. 2004a). The roughness and displacement heights, as well as the friction velocity of the logarithmic profile above a canopy have been parameterized using characteristics of the vegetation (*e.g.* Kaimal and Finnigan 1994, Luhar et al. 2008, and references therein). A number of studies have proposed models for the full velocity profile, *i.e.* both within and above the bed. These studies utilize three general approaches: (i) simple momentum balances that segregate the flow into a vegetated layer of depth h and an overflow of depth H-h (*e.g.* Stone 2002, Huthoff 2007, Cheng 2011); (ii) analytical descriptions using an eddy viscosity model, ν_t, to define the turbulent stress (*e.g.* Meijer 1998, Baptiste 2007, Poggi 2009); and (iii) numerical models with first- or second-order turbulence closures (*e.g.* Shimizu & Tsujimoto 1994, Lopez & Garcia 2001, Rowinski 2002, Neary 2003, Defina & Bixio 2005). Some of the models reflect the bending response of flexible vegetation, by solving iteratively for the meadow height and velocity profile

(Dikstra & Uittenbogaard 2010, Luhar and Nepf 2012).

4. Emergent canopies of finite width and length

The previous section described the flow near a submerged canopy that was fully developed and uniform in the horizontal plane. While the fully developed case is important, it is not representative of all field conditions. For meadows of finite width and length, the regions of flow transition at the boundaries must also be understood. A few recent studies have begun to describe the flow structure near the leading and trailing edges of a meadow; at the edges of long meadows; and within the gaps between meadows (*e.g.*, Sukhodolov and Sukhodolova, 2010, Neumeier, 2007; Folkard, 2011; Zong and Nepf, 2010; Siniscalchi et al 2012). In this section, we consider geometries that are finite in length and width. We begin with emergent canopies, *i.e.* the plant occupies the full water depth.

4.1 Long emergent canopies of finite width

In river channels, emergent vegetation often grows along the bank, creating long regions of vegetation of finite width b (Figure 3). This configuration is geometrically similar to a submerged meadow of height h (= b). Long patches of vegetation may also exist at the center of a channel, and to recognize the geometric similarity with bank vegetation, we define b as the half-width for in-channel vegetation (Figure 4). Let the stream-wise coordinate be x, with $x = 0$ at the leading edge. The lateral coordinate is y, with $y = 0$ at the side boundary for bank vegetation (Figure 3), or at the centerline for in-channel vegetation (Figure 4). The streamwise and lateral velocity are (u,v), respectively. Because the vegetation provides such high drag, relative to the bare bed, much of the flow approaching the patch from upstream is diverted away from the patch. The diversion begins upstream of the patch over a distance that is set by the scale b, and it extends a distance x_D into the vegetation (Zong and Nepf, 2010). Rominger and Nepf (2011) show that x_D scales with the larger of the two length-scales b or $L_c = 2(C_D a)^{-1}$. It is only after the diversion is complete ($x > x_D$), that the shear layer with KH vortices develops along the lateral edge of the vegetation. As discussed above, similar structures form at the top interface of submerged vegetation, and, as also noted for submerged meadows, the KH vortices at the edge of emergent meadows dominate the mass and momentum exchange between the vegetation and the adjacent open flow (White and Nepf 2007).

The initial growth and the final scale of the horizontal shear-layer vortices and their lateral penetration into the patch, δ_L, are depicted in Figure 3. The shear layer vortices extend into the open channel over the length-scale δ_o. White and Nepf (2007) show that $\delta_o \sim H/C_f$, where H is the flow depth and C_f is the bed friction. There is no direct relation between δ_L and δ_o. As expected from the discussion of vertical canopy-shear layers, $\delta_L \sim (C_D a)^{-1}$. However, the scale factor observed for lateral shear-layers (denoted by subscript L) is twice that measured for vertical shear layers above submerged meadows (δ_e, Figure 2, eq. 12). Based on White and Nepf (2007, 2008)

$$\delta_L = \frac{0.5 \pm 0.1}{C_D a} \qquad (13)$$

The difference between δ_L and δ_e may be due to the difference in flow geometry relative to the model canopy. Specifically, in experiments with vertical circular cylinders (as in White and Nepf 2007), the cylinder presents a different geometry to vortices rotating in the horizontal plane than to vortices rotating in the vertical plane. Also note that a wider range of canopy morphology, including field measurements with real vegetation, and a wider range of flow speeds were used to determine the scale factor for δ_e (Nepf et al. 2007). The scale factor for δ_L is based only on one set of flume experiments with rigid circular cylinders. Whether, or not, the difference in the scale factor is significant for field conditions has not yet been determined.

The adjustment of the flow field to a long-patch of vegetation depends on two length-scales: patch width, b, and canopy drag, $L_c \approx 2(C_D a)^{-1}$. Together they form a dimensionless parameter, $C_D ab$, called the flow blockage. Note its similarity with the roughness density (ah). A transition in flow behavior occurs at the value $C_D ab = 2$ (Rominger and Nepf 2011). According to (13), if $C_D ab > 2$ (high flow blockage), the patch width, b, is greater than the penetration distance, δ_L, and the patch is segregated into two regions: an outer region ($y > b - \delta_L$) within which the KH vortices contribute to turbulent momentum exchange, and an inner region ($y < b - \delta_L$) with negligible turbulent stress. Because turbulent stress does not penetrate to the core of a high flow blockage patch, the velocity within the patch (U_1, Figure 3) is set by a balance of potential gradient (bed and/or water surface slope) and vegetation drag. In contrast, for patches of low flow blockage ($C_D ab < 2$), U_1 is set by the balance of turbulent stress and vegetation drag. Detailed formulations for U_1 under high and low flow blockage conditions are given in Rominger and Nepf (2011).

In addition to producing turbulent momentum flux, the KH vortices also induce a pressure response. Specifically, the center of each vortex is a point of low pressure, which, for shallow flows, induces a wave response across the entire patch, and specifically beyond δ_L from the edge (White and Nepf 2007, 2008). The wave response within the vegetation has been shown to enhance the lateral (y) transport of suspended particles, above that predicted from stem-turbulence alone (Zong and Nepf 2011). For in-channel patches, shear-layers develop along both flow-parallel edges producing a train of coherent vortices along each edge (Figure 4a), and observations indicate that these vortices interact across the canopy width. The low-pressure core associated with each vortex produces a local depression in the water surface, such that the passage of individual vortices can be recorded by a surface displacement gage. A time record of surface displacement measured on opposite sides of a patch (A1 and A2 in Figure 4b) show that there is a half-cycle phase shift (π radians) between the vortex streets that form on either side of the patch. Because the vortices are a half-cycle out of phase, when the pressure (surface displacement) is at a minimum on side A1, it is at a maximum at side A2. The resulting cross-canopy pressure gradient induces a transverse velocity within the canopy (Figure 4b) that lags the lateral pressure gradient by $\pi/2$, *i.e.* a ¼ cycle. The synchronization of the vortex streets occurs even when the vortex penetration is less than the patch width, $\delta_L/b < 1$, or $C_Dab > 2$ (high flow blockage), and it significantly enhances the vortex strength and the turbulent momentum exchange between the open channel and vegetation (Rominger and Nepf 2011). More importantly, the vortex interaction introduces significant lateral transport at the center of the patch. For example, the data shown in Figure 4b corresponds to a patch with upstream flow U_o = 10 cms^{-1} and centerline velocity U_1 = 0.5 cms^{-1}. The lateral velocity at the centerline (induced by the vortex pressure field) was nearly one order of magnitude larger, with maximum lateral velocities of 3.5 cm s^{-1} (v_{rms} = 2.2 cm s^{-1}, Figure 4b). Using the period of the vortex passage (T = 10 s), the lateral excursion of a fluid parcel during each vortex cycle is 10 cm (= $v_{rms}T/2$). This lateral excursion is comparable to the half-width of the patch, b = 10 cm, indicating that fluid parcels in the center of the patch can be drawn into the free stream and vice versa, during each vortex passage. This cycle of flushing can significantly reduce the patch retention time, and may even control it. This is especially true when the aspect ratio of the canopy is greater than one, which is typical in channel vegetation, *e.g.* Sand-Jensen and Pedersen (2008) report typical length-to-width aspect ratios of 2.5. The reduced retention time has implications for plant fecundity, structural stability, and habitat viability, and the transport and fate of pollutants and contaminants.

4.2. Circular patches of vegetation

A circular patch with diameter *D* (Figure 5) is used as a model for a vegetated region with length and width smaller than the channel width. We still consider patches that are emergent, so that the flow field is roughly two-dimensional (*x*-*y*). Because the patch is porous, flow passes through it, which alters the wake structure relative to a solid body (Castro 1970, Chen and Jirka 1995, Ball et al. 1996, Takemura and Tanaka 2007). In the wake of a solid body, there is a region of recirculation directly behind the body, followed by a von Karman vortex street. The wake-scale mixing provided by the von Karman vortices allows the velocity in the wake to quickly return (within a few diameters) to a velocity comparable to the upstream (U_o). In contrast, the wake behind a porous obstruction (patch of vegetation) is much longer than that behind of solid body, because the flow entering the wake through the patch (called the bleed flow), delays the onset of the von-Karman vortex street. The velocity at the centerline of the wake, U_1, remains nearly constant over the distance from the patch to the onset of the von Karman street. This distance, L_1, is called the steady wake (Figure 5). The steady wake is a region of reduced velocity and turbulence, relative to the adjacent bare bed, so that it is a region where deposition is likely to be enhanced. The connection between the steady wake and deposition is described further in section 6.

The delayed onset of the von Karman vortex street can be visualized using traces of dye injected at the outermost edges of the patch. This is shown schematic in Figure 5. Because the steady wake is fed only by water entering from upstream through the patch, there is no dye in this region, *i.e.* the steady wake appears as a clear region directly behind the patch, in between the two dye streaks. After distance L_1, the two dye streaks come together, and a single, patch-scale, von-Karman vortex street is formed. Note that Figure 5 represents a single snapshot in time, capturing one phase of the unsteady vortex cycle. As the vortex cores migrate downstream, the flow field at any fixed point oscillates with frequency, *f*, which is set by the patch-scale *D*. The patch-scale vortex street follows the same scaling as a solid body, with Strouhal number $St = fD/U_o \approx 0.2$ (Ball et al 1996, Zong and Nepf 2012).

Near a porous patch there are two distinct regions of elevated turbulence. First, there is a peak in turbulence within and directly behind the patch, associated with the stem-scale turbulence generated in the wakes of individual stems. However, these small eddies die out quickly with distance from the patch, so that the steady wake is a region of low turbulence. A second maximum in *TKE* appears with the formation of the patch-scale vortices. The magnitude of turbulence in this second peak increases with increasing flow blockage (Zong and Nepf 2012).

Both U_1 and L_1 can be predicted from the flow blockage, which is defined as C_DaD for the circular patch geometry (Chen et al. 2012). Recognizing that $D = 2b$, we expect that for a circular patch there is a transition in flow behavior near $C_DaD = 4$. This transition is apparent in the dependence of U_1 on C_DaD (Figure 5). For low flow blockage (small C_DaD), U_1/U_o decreases linearly with C_DaD. Using $C_D = 1$, a reasonable linear fit is,

$$\frac{U_1}{U_o} = 1 - [0.33 \pm 0.08] C_D a D \tag{14}$$

For high flow blockage, U_1 is negligibly small ($U_1/U_\infty \approx 0.03$), but not zero. However, at some point around $C_DaD = 10$, U_1 becomes zero, and the flow field around the porous patch is identical to that around a solid obstruction (Zong and Nepf, 2012; Nicolle and Eames, 2011). This transition is also seen in the length-scale, L_1, discussed below.

The flow in the steady wake (U_1) separates two regions of faster velocity (U_2), creating a shear layer on either side of the steady wake. These layers grow linearly with distance from the patch (depicted by thin lines in Figure 5), eventually meeting at the wake centerline. When the shear layers meet, they interact to form the von Kármán vortex street. Thus, L_1 may be predicted from the growth of the linear shear layers. Based on this Zong and Nepf (2012) derived,

$$\frac{L_1}{D} = \frac{1}{4S_1}\frac{(1+U_1/U_2)}{(1-U_1/U_2)} \approx \frac{1}{4S_1}\frac{(1+U_1/U_o)}{(1-U_1/U_o)} \qquad (15)$$

S_1 is a constant (0.10±.02) across a wide range of D and ϕ (Zong and Nepf, 2012). If the channel width is much greater than the patch diameter, we may assume that $U_2 \approx U_O$, resulting in the right-most equation in (15). Predictions for L_1/D based on (14) and (15) do a good job representing the observed variation in L_1 with C_DaD (Figure 4b). Note that even as the velocity behind the patch approaches zero, the delay in the vortex street persists, with $L_1/D = 2.5$. However, when C_DaD becomes high enough that there is no bleed flow ($U_1 = 0$), the wake resembles that observed for a solid body, with a recirculation zone and vortex street forming directly behind the patch, so that $L_1 \approx 0$. The data shown in Figure 6 suggests that this occurs for $C_DaD > 10$. Nicolle and Eames (2011) also observed this transition in numerical simulations. Based on Figure 10 of their paper, the wake resembles that of a solid-body for $\phi \geq 0.22$, with $D/d = 21$, $C_D = 1.6$ (based on information given in *Nicolle and Eames*, 2011), so that their transition corresponds to $C_DaD = (4/\pi) C_D\, \phi\, (D/d) = 9$. This is consistent with the transition inferred from the data set shown here (Figure 6).

The wake transition described above has implications for the characterization of drag contributed by finite patches. As noted by Folkard (2010), drag is produced at two distinct scales; the leaf and stem scale, and the patch scale. For low flow blockage patches, there is sufficient flow through the patch that the stem and leaf scale drag dominates the flow resistance, *i.e*. the flow resistance can be represented by the integral of C_Dau^2 over the patch interior, with u the velocity within the patch. However, for high flow blockage patches, there is negligible flow through the patch, and the integral of $C_D a u^2$ over the patch interior is irrelevant. As revealed by the wake structure, the flow response to a high flow-blockage patch is essentially identical to the flow response to a solid obstruction of the same patch frontal area, A_p. Thus, the flow resistance provided by the patch should be represented by the patch-scale geometry, *i.e.* $C_D A_p U^2$, with U the channel velocity. This idea is supported by measurements of flow resistance produced by sparsely distributed bushes (Righetti and Armanini 2002, Righetti 2008). A bush consists of a distribution of stems and leaves, and so is a form of vegetation patch. The flow resistance generated by the bushes, D_B, was shown to fit the model, $D_B = \rho C_D A_p U^2$, and notably C_D was O(1), simlar to a solid body. Thus, although porous, the bush generated drag that was comparable to that of a solid object of the same size (A_P). It is worth noting that C_D decreased somewhat (from 1.2 to 0.8) as the channel velocity increased. This shift is most likely due to the reconfiguration of stems and leaves that reduced A_P. Since this reconfiguration was not accounted for in the analysis, it shows up as an apparent decrease in C_D. More studies are needed to explore the transition between flow resistance dominated by stem (leaf) -scale drag to flow resistance dominated by patch-scale drag. In the next section, we consider flow resistance at the channel reach scale, and again find that patch-scale geometry is more important than leaf-scale geometry.

5. Reach scale hydraulic resistance –

Field studies by Green (2005b) and Nikora et al. (2008) suggest that at the scale of the channel reach, flow resistance due to vegetation is determined primarily by the blockage factor, B_X, which is the fraction of the channel cross-section blocked by vegetation. For a patch of height h and width w in a channel of width W, and depth H; $B_x = wh/WH$. The studies show strong correlations between B_x and Manning roughness coefficient, n_M, noting that the relationship between n_M and B_x is nonlinear. These observations are in agreement with Ree (1949) and Wu et al. (1999), who showed that roughness in channels lined with vegetation is influenced primarily by the submergence ratio, H/h. For vegetation that fills the channel width, $B_x = h/H$. Luhar et al. (2008) presented a momentum balance model that explains the nonlinear relationship between n_M and B_X. However, a few studies suggest that in addition to the total flow blockage (B_x), the vegetation distribution may also influence the resistance, and specifically that greater resistance is produced by distributions with a greater interfacial area between vegetated and unvegetated regions (*e.g*. Vereecken et al. 2006, Bal et al. 2011). Luhar and Nepf (2012) quantified the impact of interfacial area by considering channels with the same blockage (B_x), but a different number (N) of patches. As the number of patches (N) increased, the length of interfacial area also increased, which led to an increase in channel resistance. However, observations made in natural rivers (Green 2006, Naden et al. 2006, Sukhodolov and Sukhodolova 2010) suggest that a realistic upper bound for the number of patches in a channel cross-section is $N = 5$, for which resistance increased by at most 20%, relative to $N = 1$. Based on this, Luhar and Nepf (2012) suggest that $N = 1$ is a reasonable simplifying assumption (with up to 20% uncertainty). Then, from momentum balance the following equations for Manning roughness can be derived.

For $B_x = 1$:
$$n_M\left(\frac{g^{1/2}}{KH^{1/6}}\right)=\left(\frac{C_D aH}{2}\right)^{1/2} \tag{17}$$

For $B_x < 1$:
$$n_M\left(\frac{g^{1/2}}{KH^{1/6}}\right)=\left(\frac{C}{2}\right)^{\frac{1}{2}}\left(1-B_x\right)^{-\frac{3}{2}} \tag{18}$$

The constant $K = 1\ \mathrm{m}^{1/3}\ \mathrm{s}^{-1}$ is required to make the equations dimensionally correct. Note that (17) is valid when $B_x = 1$, which indicates that vegetation covers the entire cross-section, width and depth. The coefficient C parameterizes the shear stress at the interface between vegetated and unvegetated regions, and $C = 0.05$ to 0.13, based on fits to field data (Luhar and Nepf 2012). While (18) seems attractively simple, remember that for flexible vegetation B_x (= wh/WH) will be a function of flow speed, because the meadow height, h, decreases as flow speed increases. To use (18) for field predictions, one needs the physical characteristics of the vegetation, specifically the buoyancy and rigidity, to estimate the meadow height, h, from equation (6).

It is instructive to consider the case of submerged vegetation that fills the channel width, such that the resistance is a function only of the submergence depth (H/h). This case has been considered in many classic papers of channel resistance, such as Ree (1949) and Wu et al (1999). For this case, the Mannings coefficient may be represented as (Luhar and Nepf 2012),

For $H/h > 1$:
$$n_M\left(\frac{g^{1/2}}{KH^{1/6}}\right) = \left[\left(\frac{2}{C}\right)^{\frac{1}{2}}\left(1-\frac{h}{H}\right)^{\frac{3}{2}} + \left(\frac{2}{C_D a h}\right)^{\frac{1}{2}}\frac{h}{H}\right]^{-1} \qquad (19)$$

If $C_D ah > C$, a common field condition, the second term drops out and (19) reverts to (18), because for vegetation covering the full channel width, $B_x = h/H$.

Several researchers have noted a non-linear relationship between n_M and a form of channel Reynolds number, VR, with V the channel average velocity and R the hydraulic radius (*e.g*. Ree 1949, Gourlay 1970). Folkard (2011) provides a useful discussion of this relationship, noting that the peak in hydraulic resistance occurs at the transition from emergent to submerged conditions. Because most channel vegetation is flexible, an increase in velocity is associated with a decrease in vegetation height, *i.e.* $h \sim 1/V$. In addition, for wide channels, $R = H$, so that $H/h \sim VR$. This suggests that the observed trends of n_M with VR can be mostly explained by the trends of n_M with H/h, as expressed through (17), for emergent conditions, and (19), for submerged conditions. As an example, n_M was calculated from (17) and (19) using $C_Dah = 10$ and $C = 0.1$ (Figure 7). If the plants are emergent ($H/h < 1$), vegetation drag increases with increasing depth ratio (H/h), because the total vegetation area per bed area (aH) increases as H/h increases (17). However, if the plants are submerged ($H/h > 1$), the hydraulic resistance decreases as H/h increases. This is made more obvious by noting that as H/h increases above 1, the second term in (19) quickly becomes negligible, reducing to $n_M = (C/2)^{\frac{1}{2}}(1 - H/h)^{-\frac{3}{2}}$. The curve shown in Figure 7 is visually similar to the many empirical curves presented for n_M versus *VR (e.g.* Ree 1949, Wu et al 1999, Folkard 2010). Finally, for flexible vegetation, we can capture the effect of reconfiguration on (19) by using the relationships discussed in section 2.2. In the terms related to flow blockage (h/H), h can be predicted from (6). In the term related to vegetation drag, C_Dah is replaced by $C_Da\,l_e$, with l_e determined from (5). The solution is iterated through predictions of n_M, U, and h and l_e until convergence.

6. Sediment transport and channel evolution

By baffling the flow and reducing bed-stress, vegetation creates regions of sediment retention (*e.g*. Abt et al. 1994, Lopez and Garcia 1998, Cotton et al. 2006, Gurnell et al. 2006). In some channels vegetation retains 80% of the sediment in transit downstream (Sand-Jensen 1998). Tal and Paola (2007) showed that single-thread channels are stabilized by vegetation. Similarly, Braudrick et al. (2009) showed that vegetation helps to maintain a meandering channel form. It is now clearly recognized that vegetation can enhance channel stability (Afzalimehr and Dey 2009; Li and Millar 2010; Wang et al. 2009, Pollen-Bankhead and Simon 2010; Wynn and Mostaghimi 2006a) and reduce sediment loading from bank erosion (Lawler 2008).

Because of the positive impacts vegetation provides for water quality, habitat and channel stability, researchers now advocate replanting and maintenance of vegetation in rivers (*e.g*., Mars et al. 1999, Pollen and Simon 2005). However, to design restoration schemes that will be sustainable, we need a better understanding of how the distribution and density of vegetation determines channel stability (Naden et al. 2006). Similarly, numerous publications (*e.g*. NRC 2002) and government policies (CBEC 2003) advocate for fluvial vegetation as traps for sediments and other pollutants, but few studies have measured actual storage rates (Noe and Hupp 2009). These gaps in understanding must be addressed through collaborations between fluvial hydraulics and geomorphology.

Most previous studies observe enhanced deposition in regions of vegetation, with greater accretion observed in regions of higher stem density (*e.g*., Bos et al. 2007). The capture of particles within regions of vegetation enhances the retention of organic matter, nutrients and heavy metals within a channel reach (*e.g*. Schultz et al., 2003; Brookshire and Dwire, 2003; Windham et al., 2003). However, some recent studies have also noted regions of erosion that develop at the edges of vegetation, because, as flow is diverted away from the vegetation, it must accelerate along the edges (Bouma et al. 2007, Rominger et al. 2010). The redistribution of flow also produces spatial patterns in sediment texture, with fine grain sediment and organic matter accumulating within patches, where velocity is reduced, and coarse grain sediment left between the patches, where velocity is enhanced (Sand-Jensen and Madsen 1992). The degree of sediment redistribution is a function of the stem density within the vegetated area (Sharpe and James 2006, Mudd et al. 2010). The opposite trend has also been observed, *i.e*. the removal of fines from within a patch. Specifically, van Katwjk et al (2010) observed that sparse patches of vegetation were associated with sandification, a decrease in fine particles and organic matter, which is most likely attributed to higher levels of turbulence within the sparse patch, relative to adjacent bare regions. If the stem density is sufficiently low, so that the velocity within the patch remains high, turbulence generation within the wakes of individual stems increases the turbulence levels within the patch (Nepf 1999), which inhibits deposition (Zong and Nepf 2012). In addition, a horseshoe vortex forms at the base of each stem (Liu et al. 2008; Nepf and Vivoni 2000), creating a local region of elevated turbulence and bed-shear stress, and producing scour holes around individual plants (Rominger et al. 2010, Figure 8), although the impact of this on spatially averaged sediment transport has not yet been described.

Elevated turbulence levels have also been observed within the leading edge of a patch, resulting in net deposition that is lower within the leading edge than in the adjacent bare bed, despite the fact that the mean flow is reduced (Zong and Nepf 2011, 2012, Cotton et al. 2006). At the same time, deposition of fine sediment has been observed in the wake behind a patch (Chen et al, 2012), which, together with the diminished deposition near the leading edge, may explain why patches grow in length predominantly in the downsteam direction (Sand-Jensen and Madsen 1992). Further, observations given in Chen et al (2012) suggest that the deposition of fine material is limited to the steady wake (L_1 in Figure 5) where both the mean and turbulent velocities are depressed. The formation of the von Karman vortex street at the end of the steady wake significantly elevates the turbulence level, inhibiting deposition. By extension, we conjecture that the onset of the von Karman vortex street may set the maximum length of enhanced deposition behind a patch, and potentially the maximum streamwise extension of a patch. The lateral growth of a patch may also be influenced by a hydrodynamic control. Specifically, the diversion of flow around a vegetated region produces locally enhanced flow at its edges that promotes erosion and inhibits its lateral expansion (Fonseca et al., 1983; Temmerman et al., 2007; Bennett et al. 2008, Bouma et al., 2009; Rominger and Nepf, 2011). These examples of the interplay between flow and patch growth demonstrate feedbacks between vegetation, flow and geomorphology. There is much to be learned about these feedbacks. Yet, this understanding is vital in the planning of successful restoration projects.

Setting aside the complexity of heterogeneous vegetation discussed above, even for homogeneous regions of uniform vegetation we lack a good description of sediment transport. This is currently hampered by two problems. First, while it is tempting to apply sediment transport models developed for open channel flow to predict sediment transport in regions of vegetation, it is not clear that this is a valid approach. Open channel flow models relate sediment transport to the mean bed stress (*e.g.* Julien 2010). However, new studies point to the important role of turbulence in initiating sediment motion (*e.g.* Nino and Garcia 1996, Papanicolaou et al. 2002, Vollmer and Kleinhans 2007, Celik et al 2010). In an open channel, the turbulence is directly linked to the mean bed stress, so that traditional sediment transport models, based on the bed shear stress, may empirically incorporate the role of turbulence into their parameterization. However, in vegetated regions, the turbulence level is set by the vegetative drag and has little or no link to the bed shear stress (*e.g.* Nepf 1999). If turbulence has any role to play in sediment transport, then we cannot expect that relationships developed for open channel flow will hold in regions with vegetation. The second problem we face in trying to characterize sediment transport within vegetation is that we lack a reliable method for predicting the mean bed shear stress within a region of vegetation. Further, there is significant spatial variability in bed stress at the scale of individual stems, *e.g.* similar to that observed around piers (Escauriaza and Sotirpoulos 2011). The spatial pattern of bed stress imposed by the stems is revealed, in part, by the scour holes observed around individual stems (*e.g.* Bouma et al. 2007). Indeed, in sand-bed rivers, the addition of vegetation can lead to a transition in bed forms, from migrating dunes to fixed patterns of scour associated with individual plants or stems (e.g. Rominger et al 2010, Figure 8). To the extent that migrating dunes contribute to sediment transport, the elimination of this migration will certainly impact bed-load transport.

6.1 Bed shear stress within a uniform canopy of vegetation

If we compare channels with and without vegetation, but with the same potential forcing, the shear stress acting on the bed, represented by the friction velocity $u_* = \sqrt{\tau_{bed}/\rho}$, is reduced in the presence of vegetation. This is reflected in the ratio $u_*\big/\sqrt{gHS}$, with S describing the slope of the bed and/or water surface. This ratio is 1 for open channel flow and less than 1 in a vegetated channel. Using a *k-ε* model to represent flow through rigid submerged vegetation (*H/h* = 3), Lopez and Garcia (1998) show that this ratio drops off steadily with increasing *aH* (and thus *ah*), approaching $u_*\big/\sqrt{gHS} = 0.1$ at $aH = 3$ ($ah = 1$). That is, the bed stress with vegetation is reduced to just 10% of the bare bed value. This dramatic reduction in bed stress is the main reason for reduced sediment transport in vegetated flow zones (Lopez and Garcia, 1998).

While it is not yet clear that sediment transport within vegetation can be predicted from bed shear stress alone, it is reasonable to expect bed stress will play a contributing role. Therefore, it is useful to consider methods for estimating this parameter in the field. Several methods for estimating bed shear stress have been developed and tested for open channel flow. However, most of these methods do not apply in the presence of vegetation, because the presence of the vegetation profoundly alters the vertical profiles of turbulence and mean flow. In the following paragraphs, we discuss five methods.

First, the bed stress is defined by the spatial average of the viscous stress at the bed,

$$\tau_{bed} = \rho {u_*}^2 = \left\langle \nu \left.\frac{\partial \overline{u}}{\partial z}\right|_{z=0} \right\rangle. \qquad (20)$$

However, to properly define $\partial\overline{u}/\partial z$ at the bed, the measurement of velocity must be within the laminar sub layer. While this is possible in a laboratory setting, it is rarely possible (or practical) to make this fine-scale measurement in the field.

Second, for open channel flow, the bed stress can be easily estimated from the maximum, near-bed Reynolds stress, or by extrapolating the linear profile of Reynolds stress to the bed (*e.g.* Nezu and Rodi, 1986). We might adapt this method to vegetated regions by imposing the spatial averaging described above, $\tau_{bed} = \rho u_*^2 = \left\langle \overline{u'w'} \right\rangle_{\max}$. However, in many vegetated flows, the near-bed turbulent stress is zero, or close to it (*e.g.* Lopez and Garcia 1998, Nepf and Vivoni 2000, Siniscalchi et al. 2012), making this estimator difficult to resolve in the field.

Third, turbulence in an open channel is produced by the boundary shear, so that there is a direct link between the bed shear stress and near-bed *TKE* ($= 0.5(\overline{u'^2} + \overline{v'^2} + \overline{w'^2})$). Observations over bare bed suggest $\tau_{bed}/\rho = u_*^2 \approx 0.2$ *TKE* (Stapleton and Huntley 1995, Rowinski et al. 2005). Although this method has been used to estimate bed stress within regions of vegetation (*e.g.* Widdows et al. 2008), it is questionable whether the method is valid over vegetated surfaces. Within vegetation, turbulence is produced predominantly in the wakes of individual stems and branches, and within the shear layer at the top of submerged meadows (section 3). There is no physical reason that τ_{bed} and *TKE* should be correlated, because the contribution of bed shear to turbulence generation within canopy is small to negligible (*e.g.* Nepf and Vivoni 2000). The lack of correlation between *TKE* and u_* is clearly demonstrated by recent measurements (F. Kerger, unpub. data). Using an LDV positioned to achieve high vertical resolution near the bed, the bed stress in a channel with rigid emergent dowels was estimated using (20). The ratio TKE/u_*^2 is plotted in Figure 9a. If an extension from open channel conditions were valid, we expect $TKE/u_*^2 \approx 5$. However, within the emergent arrays, TKE varies between 3 and 67, showing no clear trend with roughness density, *ah*.

This suggests that the estimator $u_*^2 = 0.2\ TKE$ is not valid within regions of vegetation.

Fourth, when vegetation is present, the total flow resistance can be partitioned between the bed stress and the vegetation drag (*e.g.* Raupach 1992). Integrating the momentum equation (8) over the flow depth, we can infer the bed stress by subtracting the vegetation drag from the total potential forcing, ρgSH. For steady, uniform flow conditions,

$$\underbrace{\tau_{bed} = \rho u_*^2}_{\text{bed stress}} = \rho gSH + \underbrace{\int_{z=0}^{h} \frac{1}{2}\frac{\rho}{n} C_D a \langle \overline{u} \rangle \left| \langle \overline{u} \rangle \right| dz}_{\text{vegetation drag}} \tag{21}$$

This method has been used by several authors (*e.g.* Nezu & Onitsuka 2001; Jordanova & James 2003, Larsen et al 2009, Schoneboom et al. 2010). The problem with this method is that the bed stress is generally much smaller than either term on the right-hand side, making this estimator prone to large errors. In addition, the method relies on accurate estimates of frontal area (a) and drag coefficient C_D. These values are not known for many plant species.

A possible new estimator for bed stress within vegetation is based on the following observations. If vegetation density is high enough ($ah > 0.1$), the velocity near the bed is vertically uniform and is set by the vegetation drag (*e.g.* Lightbody and Nepf 2006, Liu et al 2008). Specifically, the velocity is set by a balance of vegetation drag and potential forcing, yielding $U_v = \sqrt{2gS/C_D a}$ (*e.g.* Nepf 2012). In some cases a velocity overshoot is observed near the bed, associated with the junction vortex at the stem base (Liu et al. 2008). For the purpose of this simple analysis, we neglect this overshoot. Because the stem turbulence has scale d, we may reasonable assume that this turbulence is damped by viscous stress near the bed within a region $z < d$. This implies that the velocity deviates from its uniform value at a distance from the bed that scales with d.

If the flow conditions within this region ($z < d$) are laminar, then we can estimate (20) using the scale $\partial u/\partial z|_{z=0} \sim U_v/d$. Then, (20) reduces to

$$u_*^2 \sim \frac{\nu U_v}{d} = \frac{\nu}{d}\sqrt{\frac{2gS}{C_D a}} \tag{22}$$

The scale relation given in (22) was verified with measurements collected in uniform arrays of rigid, emergent cylinders. For simplicity, U_v is approximated by the depth-averaged velocity, U. In both studies (Zavistoski 1992, F. Kerger, unpublished data) the friction velocity was estimate from multiple vertical profiles using (20). For arrays of sufficient density ($ah > 0.1$), a consistent scale factor is suggested by the observations, $u_*^2 = [2.0 \pm 0.2]\nu U_v/d$. However, note that the data shown are limited to conditions with $Re_d < 1000$ and $Re_H < 15{,}000$, which covers only a small fraction of field conditions. Also, Ishikawa et al. (2003) directly measured the stress on a mobile bed within a region of circular cylinders, and they observed that the skin friction increased with increasing cylinder density, probably because the viscous region near the bed is thinned as the stem-generated turbulence becomes more vigorous. This implies that the scale factor in (22) may be a function of a. Clearly, more work is needed to understand the applicable limits of (22).

We conclude from the above review that there is much work needed to understand sediment transport within regions of vegetation. We lack a reliable method for estimating bed stress, and frankly, we are not even sure that the mean bed stress is the sole relevant parameter (*e.g.* Vollmer and Kleinhans 2007). We must also consider the role of turbulence (*e.g.* Nino and Garcia 1996, Celik et al 2010), and relevant to this, the turbulent structure in regions of vegetation is quite different from that over bare bed (*e.g.* Nepf 1999, 2000, Poggi et al. 2004a). Finally, the bed stress varies at the stem-scale, and this variability may play a role in setting the rates of sediment transport.

7. Conclusion and Future Directions:

This paper has covered a lot of ground, and still it has not touched on many important areas, including: the interaction of waves with submerged and emergent grasses (*e.g*. Kobayashi et al 1993, Mendez and Losada 2004, Lowe et al. 2005, Bradley and Houser 2009); the impact of vegetation on mass transport at the meadow and reach scales (*e.g*. Harvey et al. 2003, Serra et al. 2004, Ghisalberti and Nepf 2005, Sukhodolova et al. 2006, Murphy et al. 2007, Tanino and Nepf 2008, Huang et al 2008); and the dispersion and capture of pollen and seeds (*e.g*. Ackerman 1997, 2000; Chambert and James 2009, Defina and Peruzzo 2010). Indeed, the volume of research in vegetation hydrodynamics has exploded in recent years, as we realize the many environmental functions are influenced by vegetation. To end, I will note three areas in which vegetation hydrodynamics can play an important role; in resource management, environmental restoration, and carbon cycling.

Restoration: River and stream restoration seeks to return ecological function and biodiversity to channels by stabilizing stream banks, improving water quality, and restoring in-stream habitat (US EPA 2000). In the US alone, over $1 billion US dollars per year are spent on river restoration projects (Bernhardt et al., 2005). Studies of previous restoration efforts point to the need for collaboration between disciplines to design sustainable projects (Wohl et al. 2005, Palmer and Bernhardt 2006), and vegetation is a central feature in many stream restoration and bank stabilization efforts. For example, Bennett et al 2002 showed that the introduction of emergent vegetation at fixed intervals, set at the estimated equilibrium meander interval, could provoke the evolution of a straight channel toward a natural state of meandering. Similarly, Larsen and Harvey (2010) explain how vegetation and sediment transport feedbacks drive landscape evolution in the Everglades. Future research should continue to explore the feedbacks between vegetation spatial distribution, flow, and landscape evolution, which is a critical component in the design of conservation and restoration strategies for many aquatic systems.

Hydraulics Resistance and Flood Management: Vegetation was historically considered only as a source of flow resistance and was frequently removed to reduce flooding. However, vegetation provides ecological services that make it an integral part of river systems that must be maintained to some extent. The trade-off between flood and ecological management underlines the need for a reliable method to predict channel resistance in the presence of vegetation. The problem is particularly pressing given that over half of the world's major river networks are regulated to manage water resources and reduce flooding (Nilsson et al. 2005), and the frequency and magnitude of storms is projected to increase due to climate change (Oki and Kanae 2006). For many years, researchers have focused on characterizing flow resistance in channels with uniform distributions of vegetation, emphasizing the drag contributed at the stem and leaf scale (*e.g.* Kouwen and Unny 1973, Kouwen 1990). However, this approach cannot work at the reach-scale, because at the reach scale vegetation is rarely distributed uniformly, and the scale and spatial distribution of patches has been shown to play an important role in the setting reach-scale flow resistance (*e.g*. section 5, and discussion in Folkard 2010, Green 2005, 2006). It is the reach-scale resistance that is most relevant for flood and watershed management. To properly address reach-scale flow resistance, we should focus efforts in two key areas. First, we need to develop and validate methods to rapidly characterize the spatial heterogeneity of vegetation at the reach scale (also noted by Folkard 2010). Some promising methods are emerging within the fields of airborne remote sensing (*e.g*. Mertes, 2002); LIDAR imaging (*e.g*. Heritage and Milan, 2009); and other high-resolution optical methods (Feurer *et al*. 2008a, b). Second, we need to understand what scale of morphologic detail is relevant in the characterization of flow resistance. Recent studies point to spatial distribution at the patch-scale, characterized by the blockage factor, as the key geometric element in characterizing drag at the reach scale (section 5). But, we do not know the scale at which patch distribution must be resolved. In other words, how sensitive is the prediction of reach-scale flow and resistance to the resolution at which vegetation distribution is described? Or, more specifically, when are gaps between patches sufficiently wide to producing channeling flow? What scale of channel must be resolved to properly model the circulation within a marsh (e.g. Lightbody et al. 2008). These questions could be addressed through a sequence of numerical experiments that examine the impact of vegetation spatial scale on mean flow. Finally, because reconfiguration impacts the meadow height, and thus the blockage factor, we must understand what level of morphological detail is needed to properly predict reconfiguration, which in turn will require more detailed measurements of plant material density and rigidity.

Blue Carbon: Salt marshes, mangrove forests, and seagrass meadows cover less than 0.5% of the seabed, but account for 50 to 70% of the carbon storage in ocean sediments (Nellemann et al. 2009). How will the size of these habitats, and their potential for carbon storage, change with sea level rise, with changes in coastal land use, changes in dam function (and its impact on sediment supply)? Can we intentional build more marsh, mangrove, and seagrass habitat? The answer to these questions will require knowledge of vegetation hydrodynamics. For example, the potential carbon capture within a seagrass meadow depends on the photosynthetic rate, which in turn depends on blade scale hydrodynamics (which sets nutrient flux) and blade/meadow scale reconfiguration (which sets the posture of the plant, and thus influences light availability). The potential to build new marsh will depend on our understanding the feedback between vegetation, flow and sediment dynamics discussed in section 6.

To conclude, the proper management of many aquatic systems depends on understanding the impact of vegetation on flow at different scales (blade, meadow, channel reach), which in turn impacts the processes that establish and maintain important ecosystems (streams, seagrasses, marshes, mangroves). Through collaborations in ecology, biology, geomorphology, and geochemistry, the field of environmental hydraulics will answer important questions in environmental management.

Acknowledgements-

Some of this material is based upon work supported by the National Science Foundation under Grant No. EAR0309188, EAR 0125056, EAR 0738352 and OCE 0751358. Any opinions, conclusions or recommendations expressed in this material are those of the author(s) and do not necessarily reflect the views of the National Science Foundation.

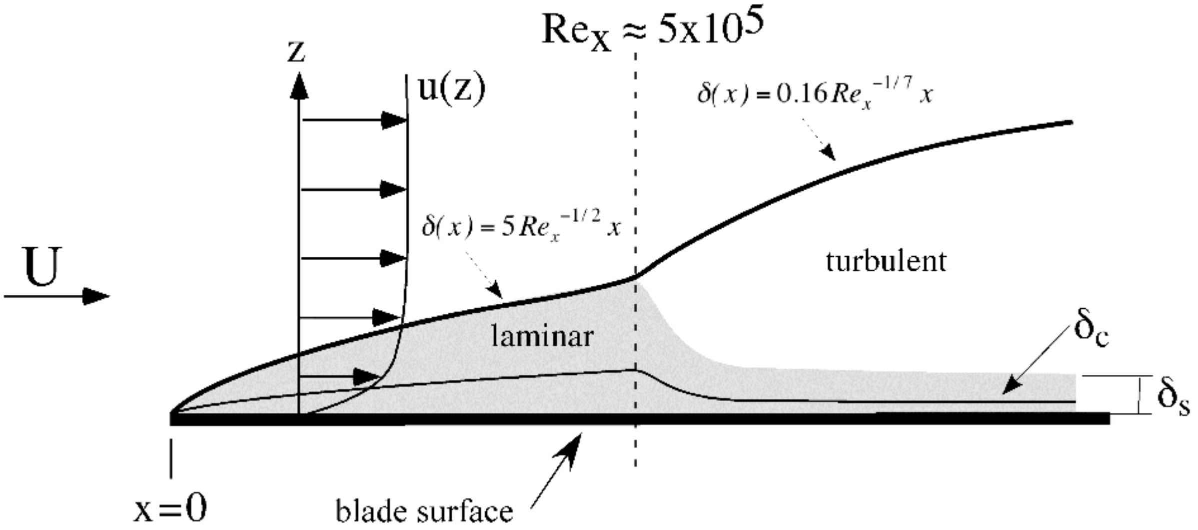

Figure 1. Evolution of a boundary layer on a flat plate. Vertical coordinate is exaggerated. The momentum boundary layer, δ, grows with distance from the leading edge ($x = 0$). Initially the boundary layer is laminar (shaded gray). At the distance, x, corresponding to $Re_x = xU/\nu \approx 5 \text{ x } 10^5$ the boundary layer becomes turbulent, except for a thin layer near the surface that remains laminar, called the viscous (or laminar) sub-layer, δ_s. In water the diffusive sub-layer, δ_c, is much smaller than the viscous sub-layer, with $\delta_c = \delta_s \text{ Sc}^{-1/3}$. Figure from Nepf (2012a).

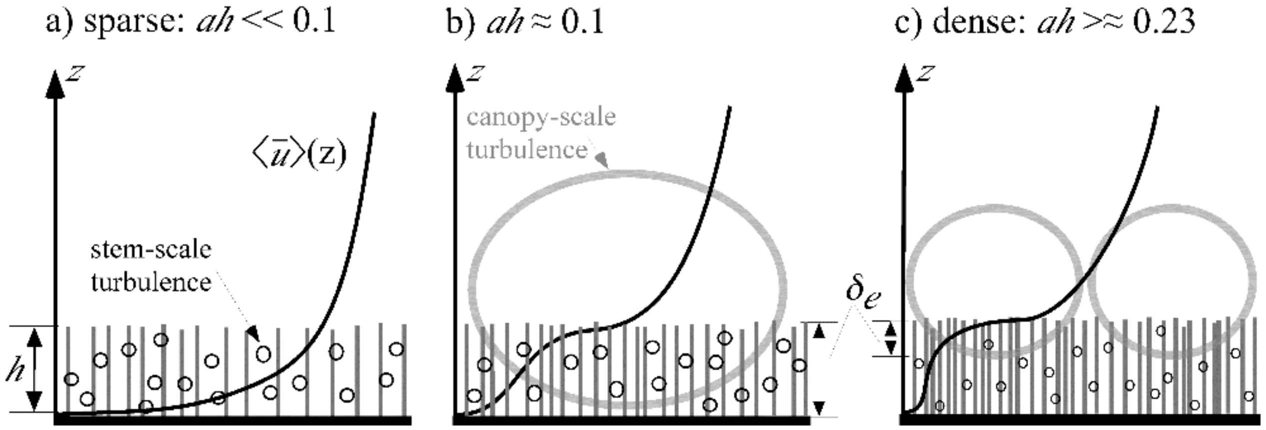

Figure 2 Changes in the mean velocity profile through a submerged meadow with increasing roughness density (*ah*). The meadow height is *h*. a) For $ah < 0.1$ (sparse regime), the velocity follows a rough boundary layer profile. b) For $ah \geq 0.1$, a region of strong shear at the top of the canopy generates canopy-scale turbulence. The canopy-scale turbulence penetrate a distance $\delta_e = [0.23 \pm 0.06](C_D a)^{-1}$ into the canopy. c) For $ah > 0.23$ (dense regime), $\delta_e < h$, and the bed is shielded from canopy-scale turbulence. Stem-scale turbulence is generated throughout the meadow. Adapted from Nepf (2012b).

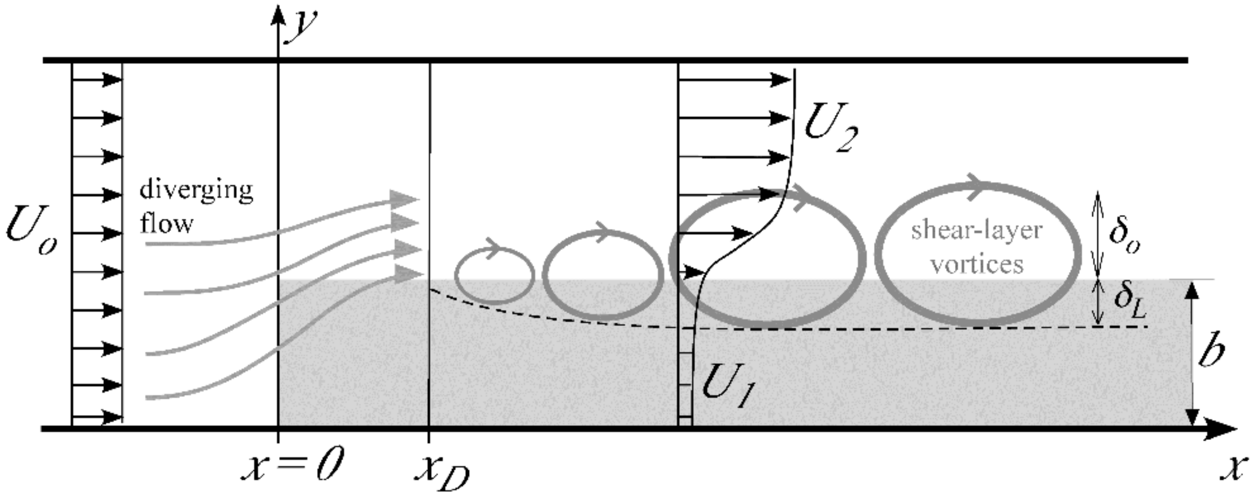

Figure 3. This is a top view of a channel with a long patch of emergent vegetation along the right bank (grey shading). The width of the vegetation zone is *b*. The flow approaching from upstream has uniform velocity U_o. The flow begins to diverge a distance *b* upstream and continues to decelerate and diverge until distance x_D. After this point, a shear layer forms on the flow-parallel edge, and shear-layer vortices form by Kelvin-Helmholtz instability. These vortices grow downstream, but subsequently reach a fixed width and fixed penetration distance into the vegetation, δ_v. Adapted from Zong and Nepf 2010.

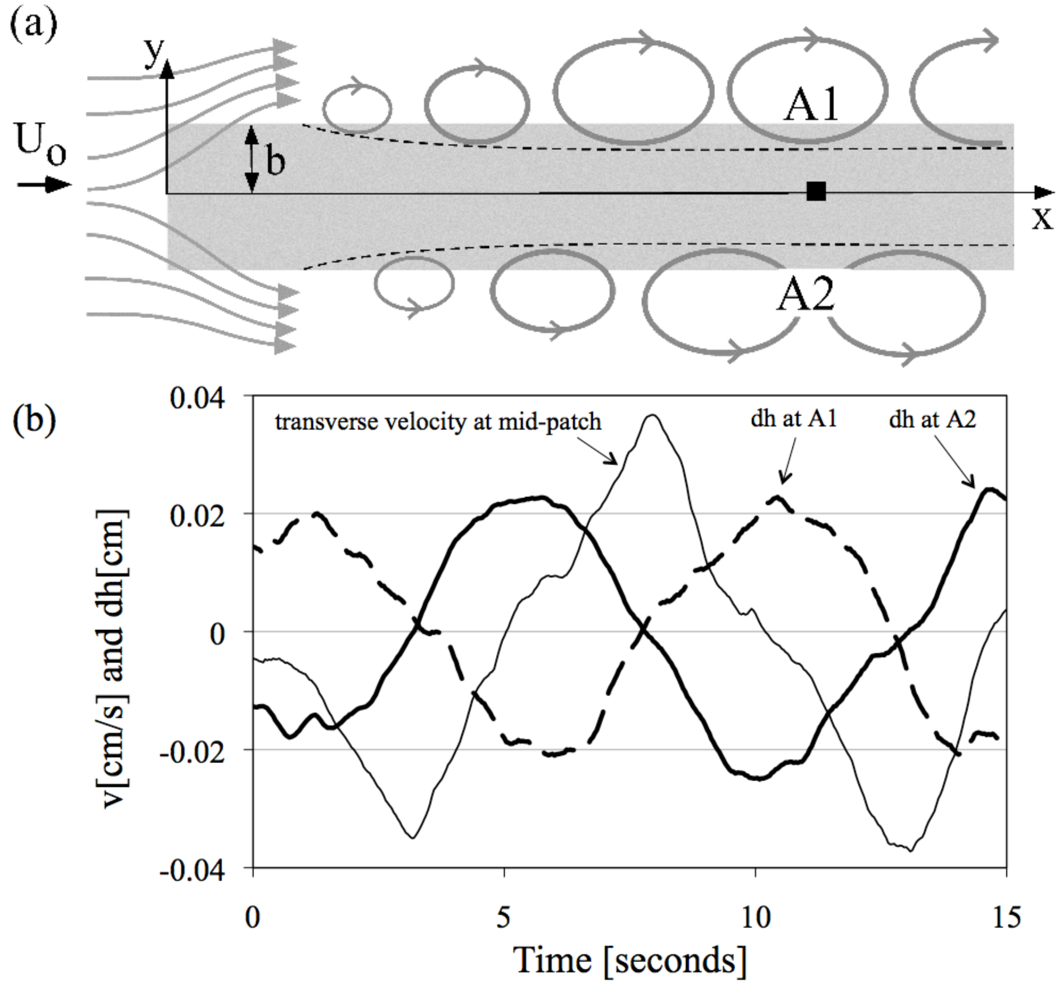

Figure 4. a) Top view of emergent vegetation with two flow-parallel edges. The patch width is 2*b*. The coherent structures on either side of the patch are out of phase. The passage of each vortex core is associated with a minimum in surface displacement, which is measured at the patch edges (A1 and A2). The velocity is measured mid-patch (square). b) Data measured with a patch of width $b = 10$ cm in a channel with flow $U_o = 10$ cms^{-1}. The patch centerline velocity is $U_1 = 0.5$ cms^{-1}. The surface displacements measured at A1 (heavy dashed line) and at A2 (heavy solid line) are a half cycle (π radians) out of phase. The resulting transverse pressure gradient imposed across the patch generates transverse velocity within the patch (thin line), which, as in a progressive wave, lags the lateral pressure gradient by a quarter cycle (π/2 radians). Adapted from Rominger and Nepf 2011.

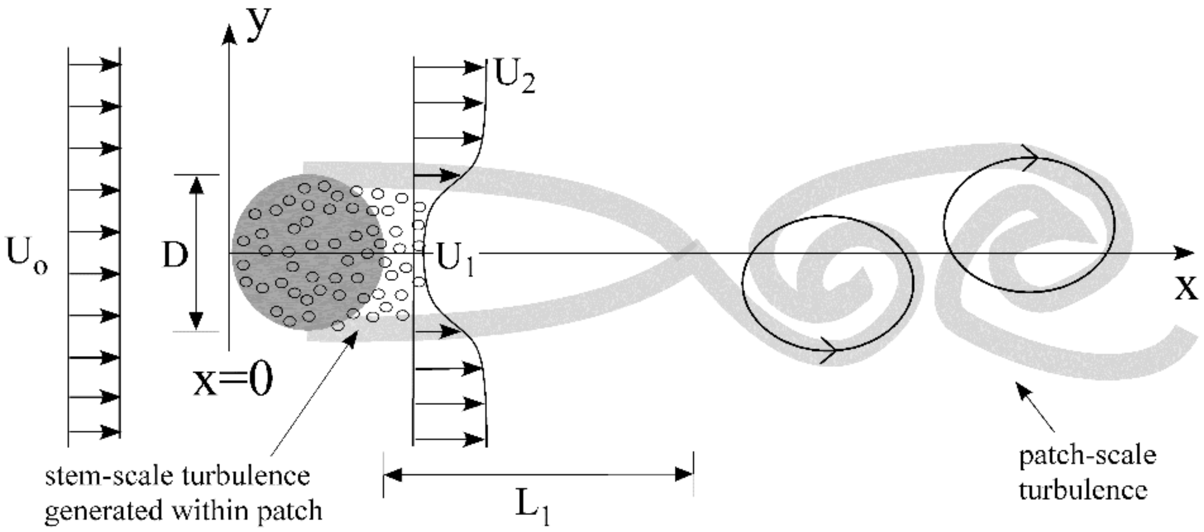

Figure 5. This is a top view of a circular patch of emergent vegetation with patch diameter *D*. The upstream, open-channel velocity is U_O. Stem-scale turbulence is generated within the patch, but dies out quickly behind the patch. Directly behind the patch is a steady wake region, with velocity U_1 at the centerline. The flow in the steady wake blocks interaction between the shear-layers at the two edges of the patch, which delays the onset of the patch-scale vortex street. Tracer (grey line) released from the outermost edges of the patch come together at a distance L_1 downstream from the patch, marking the end of the steady wake region.

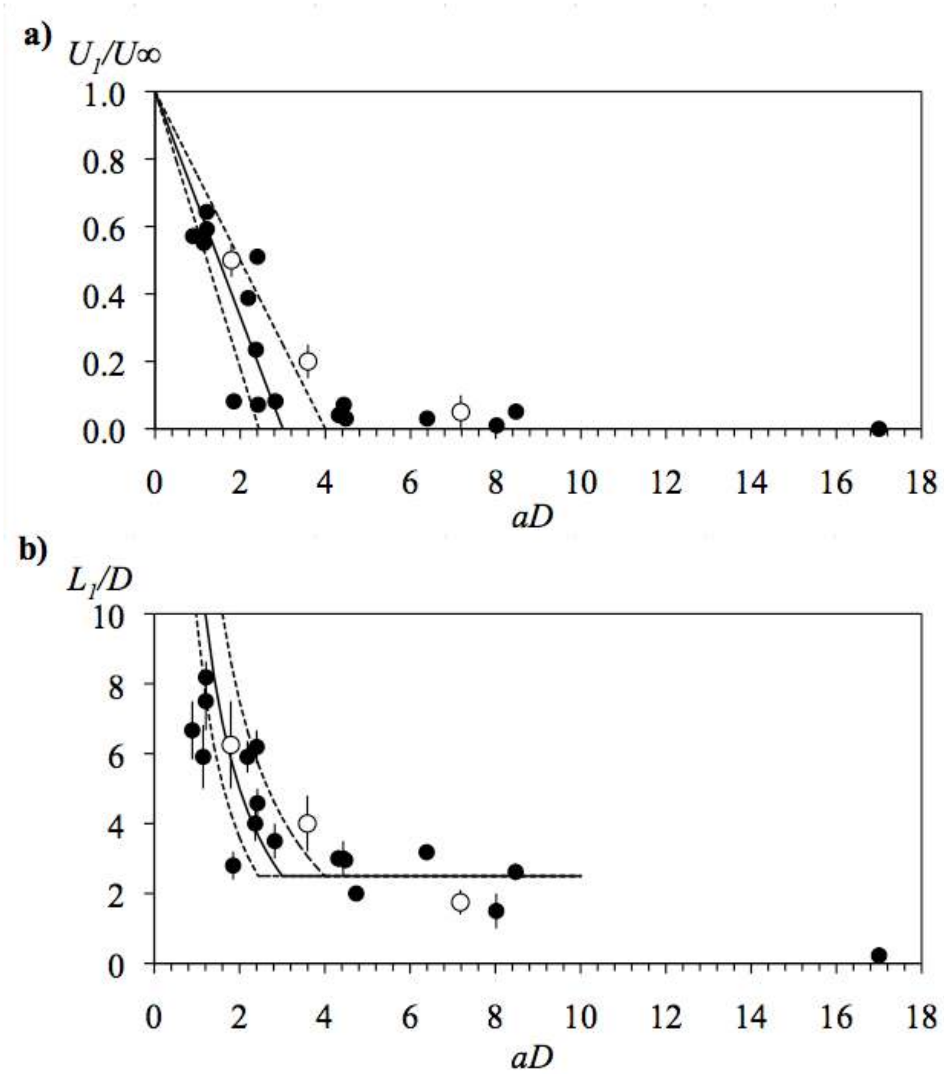

Figure 6. The flow blockage determines a) the velocity within the steady wake, U_1, and b) the length of the steady wake, L_1. a) For low flow blockage, the velocity ratio, U_1/U_o, fits a simple, linear relationship (eq. 14, shown with solid and dashed (S.D.) lines). For high flow blockage, the exit velocity is a small fraction of U_1, but non-zero, until $aD > 10$, at which point U_1 is indistinguishable from zero. b) For low flow blockage L_1 can be predicted from equations eq. (14) and (15), and becomes constant ($L_1/D = 2.5$) for high flow blockage. Model predictions are shown by black lines. Black circles measured with a circular array of circular cylinders (Chen at al. 2012). White circles measured with a square array of circular cylinders (Ball et al. 1996).

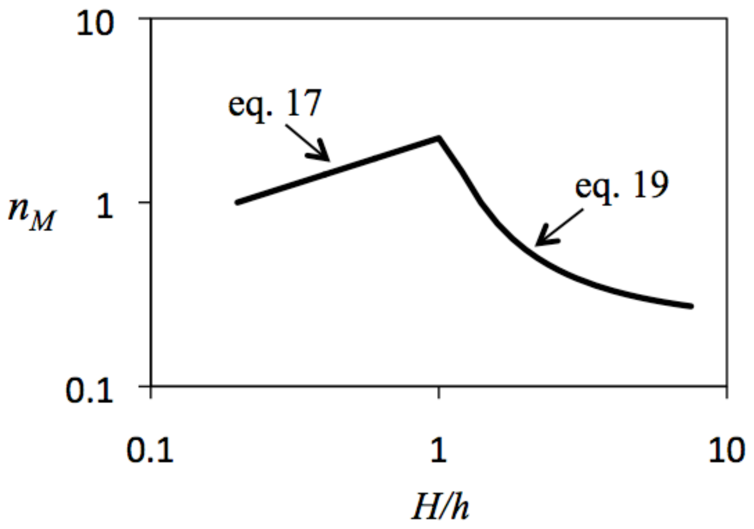

Figure 7. Mannings coefficient versus depth ratio (*H*/*h*). Most channel vegetation is flexible, so that increasing velocity is associated with a decrease in vegetation height (*h*), i.e. $h \sim 1/V$, and the previously noted non-linear trend of n_M with *VR* (e.g. Ree 1949) is captured by the trends of n_M with *H*/*h*, as expressed through (17), for emergent conditions, and (19) for submerged conditions. Based on Luhar and Nepf (2012).

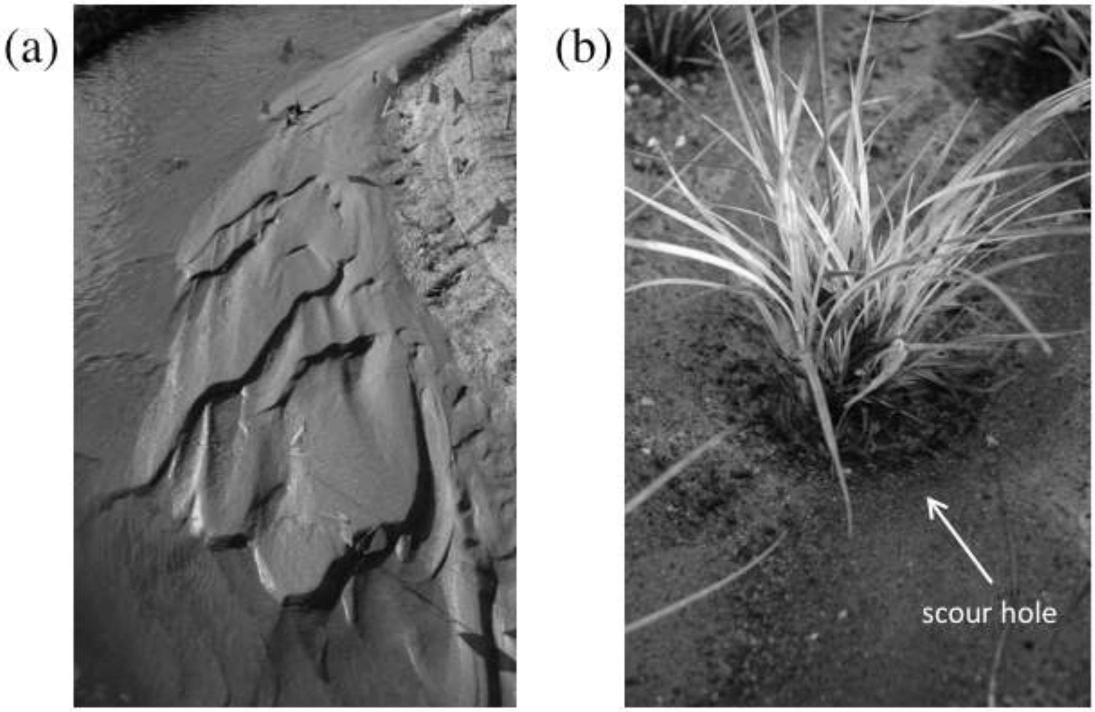

Figure 8. In a sand-bed river, the addition of vegetation to the point bars leads to a transition in bed form, from (a) migrating dunes to (b) a fixed patterns of scour associated with individual plants. Images taken by Jeff Rominger during the Outdoor StreamLab experiment at Saint Anthony Falls Laboratory 2008 (Rominger et al 2010).

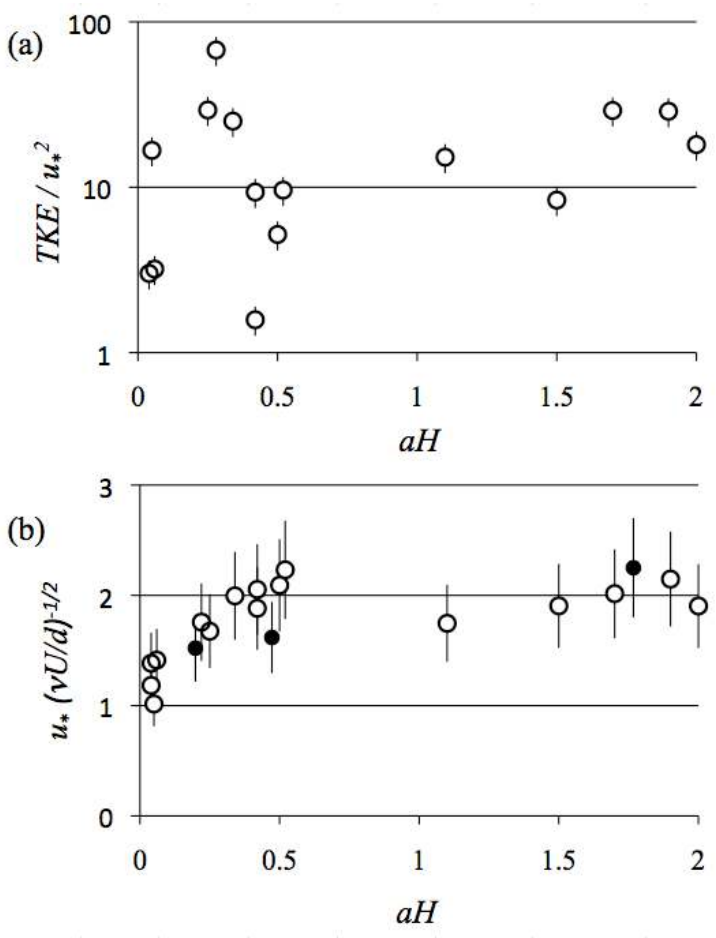

Figure 9. Measurements of bed stress in an array of emergent, rigid cylinders. Friction velocity estimated from spatial average of near-bed viscous stress, *i.e*. (20). White circles from F. Kerger (unpublished data). Black circles from Zavistoski (1992). a) Ratio of TKE to bed stress. Over a bare bed this ratio is 5 (*e.g*. Stapleton and Huntley 1995). b) Bed friction velocity normalized by bed stress estimator, as in (22). For sufficiently dense array, the ratio has a constant value.

Literature Cited

Abdelrhman, M. (2007). Modeling coupling between eelgrass Zostera marina and water flow. *Mar Ecol-Prog Ser* 338, 81–96, doi:10.3354/meps338081.

Abt, S., Clary W., Thornton, C. (1994). Sediment deposition and entrapment in vegetated streambeds. *J. Irrig Drain E-ASCE* 120 (6), 1098-1110.

Ackerman, J. (1997). Submarine pollination in the marine angiosperm *Zostera marina*. *Am J Bot* 84 (8), 1110-1119.

Ackerman, J. (2000). Abiotic pollen and pollination: ecological, functional, and evolutionary perspectives. *Plant Syst Evol* 222, 167-185.

Afzalimehr, H., Dey, S. (2009). Influence of bank vegetation and gravel bed on velocity and Reynolds stress distributions. *Int. J. Sediment Res*. 24 (2), 236-246.

Alben, S., Shelley, M., Zhang, J. (2002). Drag reduction through self-similar bending of a flexible body. *Nature* 420, 479-81.

Bal, K., Struyf, E., Vereecken, H., Viaene, P., De Doncker, L., de Deckere, E., Mostaert, F., Meire, P. (2011). How do macrophyte distribution patterns affect hydraulic resistances? *Ecol Eng* 37 (3), 529–33.

Ball, B. J., Stansby, P. K., Alliston, N. (1996). Modeling shallow water flow around pile groups. *PI Civil Eng-Water*, *118*, 226-236, doi: 10.1680/iwtme.1996.28987.

Baptist, M.J., Babovic V., Uthurburu J.R., Keijzer M., Uittenbogaard R.E., Mynett A., Verwey, A. (2007). On inducing equations for vegetation resistance. *J Hydraulic Res.* 45(4), 435–50.

Belcher, S., Jerram, N., Hunt, J. (2003). Adjustment of a turbulent boundary layer to a canopy of roughness elements. *J Fluid Mech.* 488, 369-98.

Bennett S., Pirim T., Barkdoll B. (2002). Using simulated emergent vegetation to alter stream flow direction within a straight experimental channel. *Geomorphology* 44, 115–126.

Bennett, S., Wu, W., Alonso, C., Wang, S. (2008). Modeling fluvial response to in-stream woody vegetation: implications for stream corridor restoration. *Earth Surf Proce Land* 33:890-909.

Bernhardt, E., M. Palmer, J. Allan, and the National River Restoration Science Synthesis Working Group. (2005). Restoration of U.S. rivers: A national synthesis. *Science* 308, 636–637.

Boudreau, B. and B. Jorgensen. (2001). *The Benthic Boundary Layer: Transport and Biogeochemistry*. Oxford; New York: Oxford University Press.

Bos, A., Bouma, T., de Kort, G., van Katwijk, M. (2007). Ecosystem engineering by annual intertidal seagrass beds: sediment accretion and modification. *Estuar. Coast Shelf S.*, 74, 344-348.

Bouma, T., van Duren, L., Temmerman, S., Claverie, T., Blanco-Garcia, A., Ysebaert, T., Herman, P. (2007). Spatial flow and sedimentation patterns within patches of epibenthic structures: Combining field, flume and modelling experiments, *Cont. Shelf Res.*, 27, 1020–1045, doi:10.1016/j.csr.2005.12.019.

Bouma, T., Friedrichs, M., van Wesenbeeck, B., Temmerman, S., Graf, G., Herman, P. (2009). Density-dependent linkage of scale-dependent feedbacks: a flume study on the intertidal macrophyte Spartina anglica. *Oikos*, 118, 260-268, doi: 10.1111/j.1600-0706.2008.16892.x.

Brampton AH. (1992). Engineering significance of British saltmarshes. *In* Saltmarshes: Morphodynamics, Conservation, and Engineering Significance, ed. JRL Allen, K Pye, Cambridge University Press, p. 115–122.

Bradley K., Houser C. (2009). Relative velocity of seagrass blades: Implications for wave attenuation in low-energy environments. *J Geophys. Res*., 114: F01004.

Braudrick, C.A., Dietrich, W.E., Leverich, G.T., Sklar, L.S. (2009). Experimental evidence for the conditions necessary to sustain meandering in coarse-bedded rivers. *PNAS*, 106(40), 16936-16941.

Brookshire, E., K. Dwire (2003). Controls on patterns of coarse organic particle retention in headwater streams. *J.N. Am. Benth. Soc.,* 22, 17–34.

Burke R, Stolzenbach K. (1983). Free surface flow through salt marsh grass. *Technical Report*. Massachusetts Institute of Technology, Sea Grant, 83-16, Cambridge, MA.

Carpenter SR, Lodge DM. (1986). Effects of submersed macrophytes on ecosystem processes. *Aquat Bot* 26, 341-70.

Castro, I.P. (1971). Wake characteristics of two-dimensional perforated plates normal to an air-stream. *J. Fluid Mech.*, 46, 599-609, doi:10.1017/S0022112071000727.

CBEC, Chesapeake Bay Executive Council (2003) *Expanded Riparian Forest Buffer Goals*. Directive 03-01. Annapolis, Maryland 21403

Celik, A., Diplas, P., Dancey, C., Valyrakis, M. (2010). Impulse and particle dislodgement under turbulent flow conditions. *Phys. Fluids* 22, 046601, doi:10.1063/1.3385433.

Chambers, P., Prepas, E. (1994). Nutrient dynamics in riverbeds: the impact of sewage effluent and aquatic macrophytes, *Water Res,* 28, 453-464.

Chambert, S., James C. (2009), Sorting of seeds by hydrochory. *River Res. Appl*., 25, 4861, doi:10.1002/rra.1093.

Chen, D., Jirka, G. H. (1995). Experimental study of plane turbulent wakes in a shallow water layer. *Fluid Dyn Res.* 16 (1), 11–41.

Chen, Z., A. Ortiz, L. Zong and H. Nepf. (2012). The wake structure behind a porous obstruction with implications for deposition near a finite patch of emergent vegetation. Submitted to *Water Resour Res.*

Cheng N. (2011) Representative roughness height of submerged vegetation. *Water Resour Res*. 47:W08517.

Clarke, S. (2002). Vegetation growth in rivers: influences upon sediment and nutrient dynamics. *Prog Phys Geog* 26(2), 159-172, doi:10.1191/0309133302pp324ra

Costanza, R., d'Arge, R., de Groot, R., Farber, S., Grasso, M., Hannon, B., Limburg, K., Naeem, S., O'Neill, R.V., Paruelo, J., Raskin, R.G., Sutton, P., van den Belt, M. (1997). The value of the world's ecosystem services and natural capital. *Nature* 387, 253-60.

Cotton, J., Wharton, G., Bass, J., Heppell, C., Wotton, R. (2006). The effects of seasonal changes to in-stream vegetation cover on patterns of flow and accumulation of sediment. *Geomorphology* 77, 320–334.

de Langre E. (2008). Effects of wind on plants. *Ann Rev Fluid Mech*, 40, 141-68, doi:10.1146/annurev.fluid.40.111406.102135

Denny, M. and L. Roberson. (2002). Blade motion and nutrient flux to the kelp, Eisenia arborea. *Biol. Bull.* 203, 1-13.

Defina, A., Bixio, A. (2005). Mean flow and turbulence in vegetated open channel flow. *Water Resour. Res.* 41, W07006, doi:10.1029/2004WR003475.

Defina, A. and P. Peruzzo (2010). Floating particle trapping and diffusion in vegetated open channel flow. *Water Resour. Res*., 46, W11525, doi:10.1029/2010WR009353.

Dijkstra J, Uittenbogaard R. (2010). Modeling the interaction between flow and highly flexible aquatic vegetation. *Water Resour Res*. 46, W12547, doi:10.1029/2010WR009246

Eckman J. (1990). A model of passive settlement by planktonic larvae onto bottoms of differing roughness. *Limnol Oceanogr* 35, 887-901.

Escauriaza, C., Sotiropoulos, F. (2011). Initial stages of erosion and bed form development in a turbulent flow around a cylindrical pier. *J. Geo. Res*., 116, F03007, doi:10.1029/2010JF001749.

Feurer, D., Bailly, J. and Puech, C. (2008a) Measuring depth of a clear, shallow, gravel-bed river by through-water photogrammetry with small format cameras and ultra light aircrafts. In *Geophysical Research Abstracts* 10, European Geosciences Union (EGU) General Assembly, 14–18 April, Vienna.

Feurer, D. Bailly, J.-P., Puech, C., Le Coarer, Y. and Viau, A. (2008b). Very high-resolution mapping of river-immersed topography by remote sensing. Prog. In Physical Geography, 32(4);403-419.

Finnigan J. (2000). Turbulence in plant canopies. *Ann. Rev. Fluid Mech*. 32:519-71

Finnigan, J., Shaw, R., Patton, E. (2009). Turbulence structure above a vegetation canopy. *J. Fluid Mech*. 637:387-424

Fitzmaurice L., Shaw, R., Paw, U. K.T., Patton E. (2004). Three-dimensional scalar microfronts in a large-eddy simulation of vegetation canopy flow. *Bound.-Layer Met*. 112:107–27.

Folkard, A. (2010). Vegetated flows in their environmental context: a review, *Proc. of Inst. of Civil Eng. – Eng. & Comp. Mechanics*, doi: 10.1680/eacm.8.00006.

Folkard, A. (2011). Flow regimes in gaps within stands of flexible vegetation: laboratory flume simulations, *Env. Fluid Mech*, 11:289-386, doi: 10.1007/s10652-010-437 9197-5.

Fonseca, M., Zieman, J., Thayer, G. (1983). The role of current velocity in structuring eelgrass (*Zostera* *marina L.*) meadows. *Estuar. Coast Shelf Sci. 17* (4), 367-380, doi:10.1016/0272-7714(83)90123-3.

Gambi, M., Nowell, A., Jumars, P. (1990). Flume observations on flow dynamics in *Zostera marina* (eelgrass) beds. *Mar. Ecol. Prog. Ser.* 61:159-69

Gao W, Shaw R, Paw U KT. (1989). Observation of organized structure in turbulent flow within and above a forest canopy. *Bound.-Layer Meteorol.* 47:349–77

Gaylord, B., Reed, D., Washburn, L., Raimondi, P. (2004). Physical-biological coupling in spore dispersal of kelp forest macroalgae. *J. Mar. Syst*. 49:19-39

Ghisalberti, M. (2000). *Mixing Layers and coherent structures in vegetated aquatic flows*. *MS Thesis*. Massachusetts Institute of Technology

Ghisalberti, M. (2005). Momentum and Scalar Transport in Vegetated Shear Flows. *PhD Thesis*. Massachusetts Institute of Technology

Ghisalberti, M. (2009). Obstructed shear flows: similarities across systems and scales. *J. Fluid Mech*. 641, 51-61

Ghisalberti, M., Nepf, H. (2002). Mixing layers and coherent structures in vegetated aquatic flow. *J. Geophys. Res.*, 107(C2), 10.1029/2001JC000871

Ghisalberti, M., Nepf H. (2004). The limited growth of vegetated shear -layers. *Water Resour. Res.* 40, W07502, doi:10.1029/2003WR002776

Ghisalberti M, Nepf, H. (2005). Mass Transfer in Vegetated Shear Flows. *Env. Fluid Mech*. 5(6): 527-51, doi10.1007/s10652-005-0419-1

Ghisalberti, M., Nepf, H. (2006). The structure of the shear layer over rigid and flexible canopies. *Env. Fluid Mech*. 6(3):277-301, doi10.1007/s10652-006-0002-4

Ghisalberti, M., Nepf, H. (2009). Shallow flows over a permeable medium: the hydrodynamics of submerged aquatic canopies. *Transport Porous Med.* 78:385-402, doi:10.1007/s11242-009-9434-x

Gosselin, F., deLangre, E., Machado-Almeida, B. (2010). Drag reduction of flexible plates by reconfiguration, *J. Fluid Mech*. 650:319-41.

Gourlay, M. (1970). Discussion of: Flow resistance in vegetated channels, by Kouwenm Unny, and Hill. *J. Irrig Drainage E-ASCE*, 96(IR3), 351-357.

Green, E.P, Short, F,T. (2003). *World Atlas of Seagrasses*, Univ. California Press, 310 pp.

Green J. (2005a). Further comment on drag and reconfiguration of macrophytes. *Freshwater. Biol*. 50, 2162-66.

Green, J. (2005b). Comparison of blockage factors in modelling the resistance of channels containing submerged macrophytes, *River Res. Applic.*, 21, 671-686

Green, J., (2006). Effect of macrophyte spatial variability on channel resistance, *Adv Water Resour.* 29, 426-438

Gray, W.G., Lee, P.C.Y. (1977). On the theorems for local volume averaging of multiphase systems. *Inter. J. Multiphase Flow.* 3(4), 333-40

Gurnell, A., van Oosterhout, M., de Vlieger, B., Goodson, J. (2006). Reach-scale interactions between aquatic plants and physical habitat: River Frome, Dorset. *River Res. App*. 22(6): 1535-1467.

Harvey, J., Conklin, M., Koelsch, R. (2003). Predicting changes in hydrologic retention in an evolving semi-arid alluvial stream, *Adv. Water. Resour*., *26*, 939-950.

Heritage, G., Milan, D. (2009). Terrestrial laser scanning of grain roughness in a gravel-bed river. *Geomorphology*, 113(2):1-11.

Huang, Y-H., Saiers, J., Harvey, J., Noe, G., Mylon, S. (2008). Advection, dispersion, and filtration of fine particles within emergent vegetation of the Florida Everglades. *Water. Resour. Res*. 44, W04408, doi:10.1029/2007WR006290.

Huang, I., Rominger, J., Nepf, H. (2011). The motion of kelp blades and the surface renewal model. *Limnol. Oceanogr*. 56(4): 1453-14562, doi:10.4319/lo.2011.56.4.1453

Hurd, C., Harrison, P., Druehl, L. (1996). Effect of seawater velocity on inorganic nitrogen uptake by morphologically distinct forms of the giant kelp *Macrocystis inregrifolia* from wave-sheltered and exposed sites. *Mar. Biol*., 126, 205-214.

Hurd, C., Stevens, C., Laval, B., Lawrence, G., Harrison, P. (1997). Visualization of seawater flow around morphologically distinct forms of the giant kelp *Macrocystis inregrifolia* from wave-sheltered and exposed sites. *Limnol. Oceanogr*, 41(1), 156-163.

Hurd, C.L. (2000). Water motion, marine macroalgal physiology, and production. *J. Phycol*. 36, 453-72.

Huthoff, F., Augustijn, D.C.M., Hulscher, S.J.M.H. (2007) Analytical solution of the depthaveraged flow velocity in case of submerged rigid cylindrical vegetation. *Water Resour Res.* 43(6), W06413.

Ishikawa, Y., Sakamoto, T., Mizuhara, K. (2003). Effect of density of riparian vegetation on effective tractive force. *J Forest Res*. 8(4), 235-246.

Jordanova, A., James, C. S. (2003) Experimental Study of Bed Load Transport through Emergent Vegetation. *J. Hydraul. Eng*. ASCE, 129 (6): 474-478.

Julien, P. (2010). *Erosion and Sedimentation.* 2nd ed., Cambridge University Press. Cambridge, United Kingdom.

Kaimal, J., Finnigan, J. (1994). *Atmospheric Boundary Layer Flows: Their Structure and Measurement*. Oxford University Press, Oxford, United Kingdom.

Kays, W., Crawford, M. (1993). *Convective Heat and Mass Transfer*. 3rd ed. McGraw-Hill, New York.

Kemp, J., Harper, D., Crosa, G. (2000). The habitat-scale ecohydraulics of rivers. *Ecol. Eng*., 16, 17-29.

Kobayashi N., Raichle A., Asano T. (1993). Wave attenuation by vegetation. *J. Waterw Port C Oce-ASCE*, 119:30-48

Koch E.W. (1994). Hydrodynamics, diffusion-boundary layers and photosynthesis of the seagrasses, *Thalassia testudinum* and *Cymodocea nodosa*. *Mar Biol*, 118, 767-76.

Koch, E. (2001). Beyond Light: Physical, Geological, and Geochemical Parameters as Possible Submersed Aquatic Vegetation Habitat Requirements, *Estuaries* 24(1), 1–17.

Koehl, M., Alberte, R. (1988). Flow, flapping, and photosynthesis of *Nereocystis luetkeana*: a functional comparison of undulate and flat blad morphology. *Mar. Biol*. 99, 435-444

Kouwen, N., T. Unny (1973). Flexible Roughness in Open Channels, *J. Hyd.* 99(HY5), 713-728.

Kouwen, N. (1990). Modern Approach to Design of Grassed Channels, *J. Irrig. and Drain*, 118, 733-743.

Kundu, P., Cohen, I. (2002). *Fluid Mechanics*. 2nd ed. Academic Press.

Lacy, J., Whllie-Echeverria, S. (2011). The influence of current speed and vegetation density on flow structure in two macrotidal eelgrass canopies. *Limnol Oceanogr: Fluids and Environments*, 1, 38–55 DOI 10.1215/21573698-1152489.

Larsen, L., Harvey, J. (2011). Modeling of hydroecological feedbacks predicts distinct classes of landscape pattern, process, and restoration potential in shallow aquatic ecosystems. *Geomorphology* 126:279–296, doi:10.1016/j.geomorph.2010.03.015.

Larsen, L., J. Harvey (2010). How vegetation and sediment transport feedbacks drive landscape change in the Everglades. *Am. Nat.* 176, E66–E79.

Larsen, L., Harvey, J., Crimaldi, J. (2009). Predicting bed shear stress and its role in sediment dynamics and restoration potential of the Everglades and other vegetated flow systems. *Ecol. Eng*. 35:1773-1785.

Lawler, D. (2008). Advances in the continuous monitoring of erosion and deposition dynamics: Developments and applications of new PEEP-3T system. *Geomorphology*, 93(1-2):17-39.

Lawson, S., McGlathery, K., Wiberg, P. (2012). Enhancement of sediment suspension and nutrient flux by benthic macrophytes at low biomass. *Mar. Ecol. Prog. Ser*. 448, 259-270, doi: 10.3354/meps09579.

Li, S., Millar, R. (2010). A two-dimensional morphodynamic model of gravel-bed river with floodplain vegetation. *Earth Surf. Proc. Land*. 36, 190-202.

Lightbody, A., Nepf, H. (2006). Prediction of velocity profiles and longitudinal dispersion in emergent salt marsh vegetation. *Limnol. Oceanogr.* 51(1), 218-28.

Lightbody, A., Avener, M., Nepf. H. (2008). Observations of short-circuiting flow paths within a constructed treatment wetland in Augusta, Georgia, USA. *Limnol. Oceanogr.,* 53(3), 1040-1053.

Liu, D., Diplas, P., Fairbanks, J., Hodges, C. (2008). An experimental study of flow through rigid vegetation. *J. Geophys. Res*., 113, F04015, doi:10.1029/2008JF001042.

Lopez, F., Garcia, M., (1998). Open-channel flow through simulated vegetation: suspended sediment transport modeling. *Water Resour. Res*. 34(9), 2341-52.

Lopez, F., Garcia, M. (2001). Mean flow and turbulence structure of open-channel flow through non-emergent vegetation. *J. Hydraul. Res*. 127, 392-402.

Lowe R., Koseff, J., Monismith S. (2005). Oscillatory flow through submerged canopies: 1. Velocity structure. *J. Geophys. Res.,* 110*,* (C10016), doi:10.1029/2004JC002788.

Luhar, M., Rominger, J., Nepf, H. (2008). Interaction between flow, transport and vegetation spatial structure. *Env. Fluid Mech.* 8(5-6), 423-39.

Luhar, M., Nepf. H. (2011). Flow induced reconfiguration of buoyant and flexible aquatic vegetation. *Limnol. Oceanogr*, 56(6), 2003-2017, doi:10.4319/lo.2011.56.6.2003

Luhar, M., Nepf, H. (2012). From the blade scale to the reach scale: a characterization of aquatic vegetative drag. Accepted. *Adv. Water. Resour*.

Mars, M., Kuruvilla, M., Goen, H. (1999). The role of submergent macrophyte *triglochin huegelii* in domestic greywater treatment. *Ecol. Eng.*, 12, 57-66.

Meijer, D.G., van Velzen, E.H. (1998). Prototype-scale flume experiments on hydraulic roughness of submerged vegetation. *Technical report*.

Mendez F., Losada I. (2004). An empirical model to estimate the propagation of random breaking and nonbreaking waves over vegetation fields. *Coast Eng*., 51:103-118.

Mertes, L. (2002). Remote sensing of riverine landscapes. *Freshwater Biol* 47, 799–816.

Mitsch, W.J, Gosselink, J.G. (1986). *Wetlands*. 2nd Ed. Van Nostrand Reinhold, 712pp

Moore KA. (2004). Influence of seagrasses on water quality in shallow regions of the lower Chesapeake Bay, *J. Coast. Res.*, 20 (Special Issue), 162-78.

Mudd, S., D'Alpaos, A., Morris, J. (2010). How does vegetation affect sedimentation on tidal marshes? Investigating particle capture and hydrodynamic controls on biologically mediated sedimentation. *J. Geophys. Res*. 110(F03029):14. doi:10.1029/2009JF001566.

Murphy, E., Ghisalberti, M., Nepf, H. (2007). Model and laboratory study of dispersion in flows with submerged vegetation, *Water Resour. Res*., 43, W05438, doi:10.1029/2006WR005229.

Naden, P., Rameshwaran, P., Mountford, O., Robertson, C. (2006). The influence of macrophyte growth, typical of eutrophic conditions, on river flow velocities and turbulence production. *Hydrol. Proc.* 20:3915-38.

Nicolle, A., Eames, I. (2011). Numerical study of flow through and around a circular array of cylinders, *J. Fluid Mech.*, *679*, 1-31, doi:10.1017/jfm.2011.77.

National Research Council (2002). *Riparian Areas: Functions and Strategies for Management*. National Academy Press, Washington, D.C.

Neary, V.S. (2003) Numerical solution of fully developed flow with vegetative resistance. *J Eng Mech ASCE* 129(5), 558–63.

Nellemann, C., Corcoran, E., Duarte, C. M., Valdés, L., De Young, C., Fonseca, L., Grimsditch, G. (Eds). (2009). *Blue Carbon. A Rapid Response Assessment. United Nations Environment Programme*, Arendal, Norway.

Nepf, H. (1999). Drag, turbulence, and diffusion in flow through emergent vegetation. *Water Res. Res.* 35:479-89.

Nepf H. (2012). Flow over and through biota. In: Treatise on Estuarine and Coastal Science. ed. E Wolanski, D McLusky, Elsevier Inc., San Diego.

Nepf, H. (2012). Flow and transport in regions with aquatic vegetation. *Ann. Rev. of Fluid Mech.*, 44:123-42, doi: 10.1146/annurev-fluid-120710-101048.

Nepf, H., Ghisalberti, M., White, B., Murphy, E.. (2007). Retention time and dispersion associated with submerged aquatic canopies, *Water Res. Res.*, 43, W04422, doi:10.1029/2006WR005362.

Nepf, H. (2000). Reply to Comment: Drag, turbulence and diffusivity in flow through emergent vegetation. *Water Resour. Res.*, 36(7): 1987-1988.

Nepf, H., Sullivan, J., Zavistoski, R. (1997). A model for diffusion within an emergent plant canopy. *Limnol. Oceanogr.* 42(8):85-95.

Nepf, H., Vivoni, E. (2000). Flow structure in depth-limited, vegetated flow. *J. Geophys. Res.* 105(28):547-57.

Neumeier, U. (2007). Velocity and turbulence variations at the edge of saltmarshes, *Cont. Shelf Res.*, 27:1046-1059, doi: 10.1016/j.csr.2005.07.009.

Nezu, I., Onitsuka, K. (2001). Turbulent structures in partly vegetated open-channel flows with LDA and PIV measurements. *J. Hydraul Res.*, 39(6):629-642.

Nezu, I., Rodi, W. (1986). Open-channel flow measurements with a laser Doppler anemometer, *J. Hydraulic Eng.- ASCE*, 112(5):335-355.

Nikora, V., McEwan, I., McLean, S., Coleman, S., Pokrajac, D., Walters, R. (2007). Double-averaging concept for rough-bed open-channel and overland flows: theoretical background. *J. of Hydraulic Engineering*, ASCE, 133(8):873-883.

Nikora, N., Nikora, V. (2007). A viscous drag concept for flow resistance in vegetated channels. [CD-ROM] Proceedings of the 32nd IAHR Congress, Venice, 1-6 July.

Nikora, V., Lamed, S., Nikora, N., Debnath, K., Cooper, G., Reid, M. (2008) Hydraulic resistance due to aquatic vegetation in small streams: field study. *J Hydraul Eng* ASCE 134(9), 1326–32.

Nilsson, C., Reidy, C., Dynesius, M., Revenga, C. (2005). Fragmentation and flow regulation of the world's large river systems, *Science*, 308, 405-408.

Nino, Y., Garcia, M. (1996). Experiments on particle-turbulence interactions in the near-wall region of an open channel flow: implications for sediment transport. *J. Fluid Mech.*, 326, 285-319.

Noe, G., Hupp, C. (2009). Retention of riverine sediment and nutrient loads by coastal plain floodplains. *Ecosystems*, 12, 728-746.

Okamoto T, Nezu I. (2009). Turbulence structure and monami phenomena in flexible vegetated open-channel flows. *J. Hydraulic Res*., 47(6), 798-810.

Oki, T., Kanae, S. (2006). Global hydrological cycles and world water resources, *Science*, 313, 1068-1072.

Othman, M.A. (1994). Value of mangroves in coastal protection. *Hydrobiologia*, 285, 277-282.

Palmer M., Bernhardt E. (2006). Hydroecology and river restoration: ripe for research and synthesis. *Water Resour Res* 42: W03S07. doi: 10.1029/2005WR004354.

Papanicolaou, A., Diplas, P., Evaggelopoulos, N., Fotopoulos, S. (2002). Stochastic incipient motion criterion for spheres under various bed packing conditions, *J. Hydrol. Eng*. 128, 369-380.

Plew, D., G. Cooper, and F. Callaghan (2008). Turbulence induced forces in a freshwater macrophyte canopy, *Water Resour. Res*., 44, W02414, doi:10.1029/2007WR006064.

Poggi, D., Porporato, A,, Ridolfi, L., Albertson, J., Katul, G. (2004a). The effect of vegetation density on canopy sub-layer turbulence. *Bound. Lay. Met.* 111:565-87.

Poggi, D,, Katul, G., Albertson, J., (2004b). A note on the contribution of dispersive fluxes to momentum transfer within canopies. *Bound. Lay. Met.* 111:615-21.

Poggi, D., Krug, C., Katul, G.G. (2009) Hydraulic resistance of submerged rigid vegetation derived from first-order closure models. Water Resour Res 45, W10442.

Pollen, N., Simon, A. (2005). Estimating the mechanical effects of riparian vegetation on stream bank stability using a fiber bundle model. *Water Resour. Res.*, 41, W07025, doi:10.1029/2004WR003801.

Pollen-Bankhead, N., Simon, A. (2010). Hydrologic and hydraulic effects of riparian root networks on streambank stability: Is mechanical root-reinforcement the whole story? *Geomorphology*, 116(3-4), 353-362.

Raupach, M., Shaw, R. (1982). Averaging procedures for flow within vegetation canopies. *Bound. Lay. Met. 22*, 79-90.

Raupach, M. (1992). Drag and drag partition on rough surfaces Bound.-Lay. Meteorol., 60(4), 375-395

Raupach, M, Finnigan, J., Brunet, Y. (1996). Coherent eddies and turbulence in vegetation canopies: The mixing-layer analogy. *Bound. Lay. Met*. 60:375-95.

Ree, W.O. (1949) Hydraulic characteristics of vegetation for vegetated waterways. *Agr Eng* 30:184–9.

Righetti, M., Armanini, A. (2002). Flow resistance in open channel flows with sparsely distributed bushes. *J. of Hydrology*, 269 (1-2):55-64.

Righetti, M. (2008). Flow analysis in a channel with flexible vegetation using double-averaging method. *Acta Geophysica*, 56(3), 801-823, doi: 10.2478/s11600-008-0032-z

Rominger, J., Lightbody, A., Nepf, H. (2010). Effects of added vegetation on sand bar stability and stream hydrodynamics. *J. Hydraul. Eng.* 136 (12), 994-1002.

Rominger, J., Nepf, H. (2011). Flow adjustment and interior flow associated with a rectangular porous obstruction. *J. Fluid. Mech.*, 680:636–659, doi:10.1017/jfm.2011.199.

Rowinski, P.M., Kubrak, J. (2002) A mixing-length model for predicting vertical velocity distribution in flows through emergent vegetation. *Hydrol Sci J* 47(6):893–904.

Rowinski, P.M., Aberle, J., Mazurczyk, A. (2005). Shear velocity estimation in hydraulic research. *Acta Geophysica Polonica*, 53(4), 567-584.

Sand-Jensen, K. (1998). Influence of submerged macrophytes on sediment composition and near-bed flow in lowlands streams, *Freshwater Biol*, 39:663-679.

Sand-Jensen K. (2003). Drag and reconfiguration of freshwater macrophytes. *Freshwater Biol*. 48:271-83

Sand-Jensen, K., Pedersen, M. L. (2008). Streamlining of plant patches in streams. Freshwater Biol. 53, 714–726.

Sand-Jensen, K., Madsen, T.V. (1992). Patch dynamics of the stream macrophyte, Callitriche cophocarpa, *Freshwater Biol.*, *27*, 277-282, doi:10.1111/j.1365-2427.1992.tb00539.x.

Schnauder, I., Moggridge, H. (2009), Vegetation and hydraulic-morphological interactions at the individual plant, patch and channel scale. *Aquat. Sci*., *71*, 318-330, doi 10.1007/s00027-009-9202-6.

Schoneboom,T., Aberle, J., Dittrich, A. (2010) CHydraulic resistance of vegetated flows: Contribution of bed shear stress and vegetative drag to total hydraulic resistance. In River Flow 2010, Braunschweig, Germany (ed. Dittrich, A. et al.), Bundesanstalt fr Wasserbau.

Schultz, M., Kozerski, H-P, Pluntke, T., Rinke, K. (2003). The influence of macrophytes on sedimentation and nutrient retention in the lower River Spree. *Water Resour. Res*., 37, 569–578.

Serra, T., Fernando, H.J.S., Rodriquez, R. (2004). Effects of emergent vegetation on lateral diffusion in wetlands. *Water Research*, 38:139-47.

Sharpe, R., James, C. (2006). Deposition of sediment from suspension in emergent vegetation. *Water SA*, 32(2): 211-218.

Siniscalchi, F., Nikora, V., Aberle, J. (2012). Plant patch hydrodynamics in streams: mean flow, turbulence, and drag forces. *Water Resour. Res*., 48, W01512, doi:10.1029/2011WR011050

Shimizu, Y., Tsujimoto, T. (1994). Numerical analysis of turbulent open-channel flow over a vegetation layer using a *k-e* turbulence model. *J. Hydrosci. Hydraul. Eng*. 11:57-67.

Stapleton, K., Huntley, D. (1995). Seabed stress determination using the inertial dissipation method and turbulent kinetic energy method. *Earth Surf. Process Land* 20, 807-815

Statzner, B., Lamouroux, N., Nikora, V., Sagnes, P. (2006). The debate about drag and reconfiguration of freshwater macrophytes: comparing results obtained by three recently discussed approaches. *Freshwater Biol*. 51:2173-83.

Stevens, C., Hurd, C., Isachsen. P. (2003). Modelling of diffusion boundary-layers in subtidal macrogalgal canopies: response to waves and currents. *Aquat. Sci*. 65, 81-91.

Stone, B.M., Shen, H.T., (2002) Hydraulic resistance of flow in channels with cylindrical roughness. *J Hydraul Eng* ASCE 128(5):500–6.

Sukhodolov A. (2005). Comment on drag and reconfiguration of macrophytes. *Freshwater Biol*. 50:194-95.

Sukhodolova, T., Sukhodolov, A., Kozerski, H., Köhler, J. (2006). Longitudinal dispersion in a lowland river with submersed vegetation. In: River Flow 2006, Int. Conf. on Fluvial Hydr., A4021, Lisbon, Portugal.

Sukhodolov, A., Sukhodolova, T. (2010). Case study: effect of submerged aquatic plants on turbulence structure in a lowland river. *J. Hydr. Eng.*, 136(7): 434-446, doi:10.1061/_ASCE_HY.1943-7900.0000195.

Takemura, T., Tanaka, N. (2007), Flow structures and drag characteristics of a colony-type emergent roughness model mounted on a flat plate in uniform flow, *Fluid Dyn. Res.*, *39*, 694-710, doi:10.1016/j.fluiddyn.2007.06.001.

Tal, M., Paola, C. (2007) Dynamic single-thread channels maintained by the interaction of flow and vegetation, *Geol Soc. Am*, 35:347-350.

Tanino, Y., Nepf, H. (2008). Lateral dispersion in random cylinder arrays at high Reynolds number. *J. Fluid Mech.* 600, 339-71.

Temmerman, S., Bouma, T.J., de Koppel, V., van der, W., de Vries, M.B., Herman, P.M.J. (2007), Vegetation causes channel erosion in a tidal landscape, *Geology*, *35*(7), 631–634, doi: 10.1130/G23502A.

Thomas, F., Cornelisen, C. and J. Zande. (2000). Effects of water velocity and canopy morphology on ammonium uptake by seagrass communities. *Ecology* 81 (10): 2704-2713.

Turker, U., Yagci, O., Kabdasli, M. (2006). Analysis of coastal damage of a beach profile under the protection of emergent vegetation. *Ocean Engineering*, 33, 810-828.

US Environmental Protection Agency (2000). *Principles for the Ecological Restoration of Aquatic Resources*, Report EPA841-F-00- 003, Office of Water (4501F), Washington, DC.

van Katwijk, M., Bos, A., Hermus, D., Suykerbuyk, W. (2010). Sediment modification by seagrass beds: muddification and sandification induced by plant cover and environmental conditions. *Estuar. Coast. Shelf Sci*., doi:10.1016/j.ecss.2010.06.008.

Vereecken, H., Baetens, J., Viaene, P., Mostaert, F., Meire, P. (2006). Ecological management of aquatic plants: effects in lowland streams. *Hydrobiologia*, 570:205-210. DOI 10.1007/s10750-006-01815

Velasco, D, Bateman, A., Redondo, J., Demedina, V. (2003) An open channel flow experimental and theoretical study of resistance and turbulent characterization over flexible vegetated linings. *Flow Turbul. Combust.* 70(1–4), 69–88.

Vogel, S. (1994). *Life in Moving Fluid* 2nd ed., Princeton University Press, Princeton, NJ.

Vollmer, S., Kleinhans, G. (2007). Predicting incipient motion, including the effect of turbulent pressure fluctuations in the bed. *Water Resour. Res*., 43, W05410, doi:10.1029/2006WR004919.

Wang, C., Yu, J., Wang, P., Guo. P. (2009). Flow structure of partly vegetated open-channel flows with eelgrass. *J. of Hydrodynamics*, *Ser.B*., 21(3): 301-307.

White, B., Nepf, H. (2007). Shear instability and coherent structures in a flow adjacent to a porous layer, *J. Fluid Mech*. 593:1-32.

White, B., Nepf. H. (2008). A vortex-based model of velocity and shear stress in a partially vegetated shallow channel. *Water Resour. Res*., 44(1):W01412, doi. 10.1029/2006WR005651

White, F.M., (2008). *Fluid Mechanics*, 6th Ed., McGraw Hill, Boston, MA, USA.

Widdows, J., Pope, N., Brinsley, M. (2008). Effect of *Spartina anglica* stems on near-bed hydrodynamics, sediment erodability and morphological changes on an intertidal mudflat. *Mar. Ecol. Prog. Ser.*, 362, 45-57.

Wilcock, R., Champion, P., Nagels, J., Crocker, G. (1999). The influence of aquatic macrophytes on the hydraulic and physicochemical properties of a New Zealand lowland stream, *Hydrobiologia*, **416**(1), 203-214.

Windham, L., Weis, J., Weis, P. (2003). Uptake and distribution of metals in two dominant salt marsh macrophytes, *Spartina alterniflora* and *Phragmites australis*, *Estuar. Coast. Shelf Sci*., 56:63–72.

Wohl, E.,Angermeier, P., Bledsoe,B.,Kondolf, G.M., Mac-Donnell, L., Merritt, D., Palmer, M., Poff, N. &Tarboton, D. (2005). River restoration. *Water Resour. Res.* 41: W10301.

Wooding, R., Bradley, E., Marshall, J. (1973). Drag due to regular arrays of roughness elements. *Bound. Lay. Met*. 5, 285-308.

Wu, F., Shen, H., Chou, Y. (1999) Variation of roughness coefficients for unsubmerged and submerged vegetation. *J Hydraul Eng* ASCE 125(9):934–42.

Wynn, T., Mostaghimi, S. (2006). Effects of riparian vegetation on stream bank subaerial processes in southwestern Virginia, USA. *Earth Surf. Proc. Landforms*. 31:399-413.

Zavistoski, R. (1992). Hydrodynamic Effects of Surface Piercing Plants. *SM Thesis.* Massachusetts Institute of Technology.

Zimmerman, R. (2003). A biooptical model of irradiance distribution and photosynthesis in seagrass canopies, *Limnol Oceanogr* 48(1): 568-585

Zong, L., Nepf. H. (2010). Flow and deposition in and around a finite patch of vegetation. *Geomorphology.* 116:363-372. doi:10.1016/j.geomorph.2009.11.020.

Zong, L. Nepf H. (2011). Spatial distribution of deposition within a patch of vegetation *Water Resour. Res*., 47, W03516, doi:10.1029/2010WR009516.

Zong, L., Nepf. H. (2012). Vortex development behind a finite porous obstruction in a channel., *J. Fluid Mech*., 691: 368-391, doi:10.1017/jfm.2011.479